Naval Research Laboratory

Washington, DC 20375-5000

NRL Memorandum Report 6661

High Power Microwaves for Defense and Accelerator Applications

WALLACE M. MANHEIMER

Senior Scientist Fundamental Plasma Processes Branch
Plasma Physics Division

June 11, 1990

REPORT DOCUMENTATION PAGE

Form Approved
OMB No. 0704-0188

1. AGENCY USE ONLY *(Leave blank)*	2. REPORT DATE	3. REPORT TYPE AND DATES COVERED
	1990 June 11	

4. TITLE AND SUBTITLE

High Power Microwaves for Defense and Accelerator Applications

5. FUNDING NUMBERS

47-2797

6. AUTHOR(S)

Wallace Manheimer

7. PERFORMING ORGANIZATION NAME(S) AND ADDRESS(ES)

Naval Research Laboratory
4555 Overlook Ave. S.W.
Washington, DC 20375-5000

8. PERFORMING ORGANIZATION REPORT NUMBER

NRL Memorandum Report 6661

9. SPONSORING / MONITORING AGENCY NAME(S) AND ADDRESS(ES)

Office of Naval Research
800 North Quincy Street
Arlington, VA 22217-5000

10. SPONSORING / MONITORING AGENCY REPORT NUMBER

ONR

11. SUPPLEMENTARY NOTES

12a. DISTRIBUTION / AVAILABILITY STATEMENT

Approved for public release; distribution unlimited.

12b. DISTRIBUTION CODE

13. ABSTRACT *(Maximum 200 words)*

This paper discusses high power microwaves for application to the Defense Department and to the powering of large accelerators. The microwave sources discussed are the SLAC klystron, the relativistic klystron, the magnetron and the vircator.

14. SUBJECT TERMS

Microwave Directed Energy Accelerators, High Power Microwave

15. NUMBER OF PAGES

75

16. PRICE CODE

17. SECURITY CLASSIFICATION OF REPORT	18. SECURITY CLASSIFICATION OF THIS PAGE	19. SECURITY CLASSIFICATION OF ABSTRACT	20. LIMITATION OF ABSTRACT
UNCLASSIFIED	UNCLASSIFIED	UNCLASSIFIED	

CONTENTS

HIGH POWER MICROWAVES FOR DEFENSE AND ACCELERATOR APPLICATIONS

1. INTRODUCTION

Virtually all microwave tubes (frequency above 1 GHz) built today are used for two customers, the department of defense and the accelerator community. For the defense department, the traditional uses are radar, communication and electronic warfare. However as the power of microwave tubes is being scaled up, new innovative applications are being suggested. These include decoy discrimination for strategic defense, and microwave directed energy. In the former, a large area, high power microwave beam is used to irradiate many missiles in their midcourse trajectory. The hope is that lightweight balloons will blow open in the intense microwave fields[1]. For directed energy, the idea is that a high power microwave beam illuminating a target will disable some sensitive electronic component and thereby disable the entire target[2,3]. For both of these potential defense department applications, the role of the microwave is very different from its traditional one. Traditionally, it is the *information* carried by the microwaves that does the job; in these new potential roles, it is the *energy* of the microwaves that does it. In that sense, the emerging defense department roles for microwaves are more like the traditional accelerator roles, that is to provide energy to a beam of charged particles. However the defense department application is inherently much more difficult because it has to beam the energy over large distances.

With the apparent outbreak of peace in the world, there is great pressure to reduce the Defense Department budget; with the problem of national deficits, there is great pressure to reduce all federal spending. Thus it seems to make sense for the defense and accelerator microwave communities to try to see whether there are common approaches and technologies to apply to each other's problems. Unfortunately, support for high power microwaves in the defense department tends to go through rapid boom and bust cycles and at any one time one can be in either phase. The most recent booms have been support from the Strategic Defense Initiative and form a new tri-service group called the Balanced Technology Initiative. The former is attempting to develop extremely high power phase locked sources, principally for decoy discrimination; and the latter is trying to develop high powered sources for tactical directed energy. For each case, the main frequency of interest is about 1-4 GHz, which is just the frequency that many large accelerators operate at. Thus, we will concentrate here on this frequency range as regards Defense Department sources. The sources to be discussed here include the SLAC klystron, the relativistic klystron, the relativistic magnetron, and the vircator. These are just the sources that the Balanced Technology Initiative recently concentrated on when considering whether to build a large scale

Manuscript approved March 19, 1990.

demonstration project. To start however, we will consider the most analogous accelerator source, the SLAC klystron, and this will serve as a basis of comparison of the capabilities in each community. As we will see, the Defense Department sources typically operate at higher voltage and current, but much shorter pulse time. Although we concentrate here on L and S-band sources here, it is worth pointing out that the high current, high voltage technology has also been utilized at higher frequency. Some specific examples are backward wave oscillators at X-band[4-7], gyrotrons[8,9], free electron lasers[10,11] and cyclotron autoresonance masers[12] at K_a-band, and free electron lasers at W-band[13]. We should also point out that there are several archival journals and books on high power microwave sources and these are excellent references. Some of these are "High Power Microwave Sources" Edited by Granatstein and Alexeff, published by Artech House: There have been two special issues of IEEE Transactions on Plasma Science which have been devoted to High Power Microwave sources. These are the December, 1985 and April, 1988 issues. Another is coming out in June, 1990. The Strategic Defense Initiative has held conferences on High Power Microwave Sources, and these are published in SPIE transactions. Two which have been published already are the SPIE Transactions Volumes 873, edited by Rostoker, and Volume 1061, edited by Brandt.

In the next section, we will begin with a discussion of the SLAC klystron. Then we will discuss the general characteristics of intense pulsed beams and their opportunities and constraints as generators of high power microwaves. After that we will discuss in turn relativistic klystrons, relativistic magnetrons, and vircators.

2.THE SLAC KLYSTRON

We begin with a review of the SLAC klystron, the klystron that powers the Stanford Linear Accelerator. Although this is not usually considered to be a high power microwave tube in the sense generally used in defense department laboratories, it provides an excellent background and contrast to the latter. As we shall see, although its power is lower, its energy per pulse is comparable to or higher than HPM sources generated by intense pulsed beams. Furthermore, its average power capability is much higher. We will follow the format of most of the sections of this review, namely will discuss several key elements of the theory of the tube and then discuss the experimental results.

A klystron has at least two cavities which the electron beam traverses. Power is injected into the first cavity, so that the beam velocity is modulated. In a drift section between the cavities, the velocity modulation is converted to a density modulation as the beam ballistically bunches when the faster electrons catch up with the slower ones. The radius of this drift section is chosen small enough that it is cut off to modes at the drive frequency. Thus there is no rf field in the drift section and the bunching of the beam is purely ballistic, although as we will see, the space charge set up by the bunched beam can ultimately limit the bunch charge density. When the beam enters the second cavity, the bunches are phased with the electric field there so that the rf field decelerates each bunch. The beam energy is then transferred to the rf fields in the cavity, which is itself extracted through some output hole in it. Typically, in klystrons, the power is extracted from the final cavity through a radial hole in the sidewall.

To examine these issues more quantitatively, let us imagine that each cavity is excited in the TM_{01} mode. Thus there is an axial electric field which serves to velocity modulate the beam in the first cavity and extract energy from the longitudinal motion in the second cavity. Thus the electric field in the first cavity, characterized by a subscript i is given by

$$E_z = E_i J_0(\omega r/c)\cos\omega t \qquad (1)$$

where at the wall r=a, the $J_0(\omega a/c) = 0$ so that $a = 2.4c/\omega$. The beam comes through a hole in the cavity at the axis so that the equation of motion of the electron in the z direction is given by

$$\gamma^3 m(dv_z/dt) = eE_i \cos\omega t \qquad (2)$$

If the initial cavity has axial length d, then the perturbed velocity, δv_z is given by

$$\delta v_z = \{eE_i d/\gamma^3 m v_z\}\cos\,\omega t_i \equiv \delta v_{z0}\cos\omega t_i$$

where t_i is the time the electron enters the input cavity and we have assumed that $\omega d/v_z << 1$.

Now let us consider the motion of the electron in the drift region. Since there is no field there, the electron motion is ballistic as long as the space charge fields can be neglected. (Incidentally the TM_{01} mode is not the lowest order mode in the cavity, the TE_{11} is. Thus the radius of the drift region is generally taken small enough so that this mode does not propagate either, or is taken less than $1.8c/\omega$.) If the second cavity is a distance L downstream from the first, the electron enters the output cavity at a time given approximately by

$$t_0 = t_i + L/v_z + \{eLE_i d/m\gamma^3 v_z^3\}\cos\,\omega t_i. \qquad (3)$$

Now let us look at the question of ballistic bunching. Consider two electrons which enter the first cavity with a time difference dt_i. Their initial separation is $v_z dt_i$. Upon exiting the cavity they have slightly different velocity given by $\delta v_{z0}\omega dt_i \sin\omega t_i$. Thus after propagation of a distance L, the separation of the electrons is $v_z dt_i - \delta v_{z0}(\omega L/v_z)dt_i \sin\omega t_i$. The relative density of the beam, as it travels is given by the reciprocal of the relative distance apart of the electrons as long as the electrons do not overtake one another. That is

$$\sigma(L)/\sigma = [1-\delta v_{z0}(\omega L/v_z^2)\sin\omega t_i]^{-1} \qquad (4)$$

Here σ is the line charge density of the beam. Thus in a distance $v_z^2/\omega\delta v_{z0}$, the density diverges, indicating that the fast particle behind the slower one has caught up and overtaken it. This then is the optimum distance between the cavities in a klystron. Notice that even if the field in the prebunching cavity is very small, implying a very small δv_z, there can still be complete bunching just by making L correspondingly large. As we will see, effects of beam temperature and space charge limit the bunching. For this reason, in practice, more than two cavities are generally used in a klystron (the SLAC klystron uses seven). Between any two cavities, the beam bunches its maximum amount depending on thermal spread or space charge. This bunched beam then excites a larger amplitude oscillation in the next cavity and the process cascades.

Let us now calculate the power loss of the beam in the output cavity, where fields are characterized by a subscript zero. The energy loss for each particle is given by minus the integral of eE_o with distance in the second cavity. Recall that the time in the second cavity is given by t_0+z/v_z. The energy loss for the total beam is given by the average over entrance time in the input cavity, which is assumed to be uniform. (Note that the entrance time into the second cavity is not distributed uniformly because the beam is bunched.) Thus the energy lost by the beam on traversing the second cavity is given by

$$W = -e(\omega/2\pi)\int dz dt_i\, E_0 \cos\,[\omega(t_i+L/v_z + \{eE_i dL/m\gamma^3 v_z^3\}\cos\omega t_i + z/v_z)+\beta] \qquad (5)$$

where β is the phase shift between the cavities and we have assumed that the second cavity has the length d_0. The integral over t_i can be expressed in terms of Bessel functions with the result:

$$W = -e \int dz\;\; E_0\, J_1(q)\cos\,[\omega(L+z)/v_z + \beta] \qquad (6)$$

where q is the so called bunching parameter $q = \omega e E_i dL/m\gamma^3 v_z^3$. The z integral is simply the integral of a cosine and it will have its maximum for $\omega d_0/v_z = \pi$. In this case,

$$W = 2e(v_z E_0/\omega)\, J_1(q)\sin(\omega L/v_z + \beta) \qquad (7)$$

The power loss maximizes for $\omega L/v_z + \beta = \pi/2$. Actually more careful analysis shows that this phase is controlled by the precise frequency at which the klystron is operated at. Notice also that there is no benefit to making the output cavity any longer than half a wavelength; the energy will just oscillate if the distance is longer. This then is one of the main constraints on klystron design at high frequency. Since the rf field on the wall is constrained by some breakdown limit, and eE_0d_0 must equal the energy of the beam, d_0 must be above some minimum value. This translates into some minimum wavelength for which a klystron can operate efficiently.

Now let us consider the effect of thermal spread on the beam. Since the cathode is generally at a particular Voltage, the beam has a single energy. However there might be a thermal spread in v_z because either there is a thermal spread in pitch angle, or else because some of the beam energy is potential energy due to for instance an electrostatic potential drop across the beam space charge. Recall that the klystron is efficient because the beam coherently bunches in the drift region. The effect of a thermal spread in v_z then is to smear out this coherence and thereby reduce the

bunching. The actual reduction of efficiency is quite easy to calculate. Simply let v_z be an independent variable and multiply the integrand of Eq.(5) by the distribution function $f(v_z)$ and integrate over v_z. If the velocity is defined as $v_{z0} + \Delta v$, where v_{z0} is the average velocity and Δv is the now the independent variable, the main effect on the phase arises from where the small velocity perturbation multiplies the drift length. That is if W_0 is the energy loss for the case of no thermal spread, the energy loss in the presence of thermal spread is given by

$$W = W_0 \exp -[\omega L \Delta v_t / 2v_0^2]^2 \qquad (8)$$

where we have assumed for Δv a Gaussian distribution having thermal spread Δv_t. Clearly, too much thermal spread on the beam ruins the interaction efficiency. Equation (8) above gives the condition for thermal spread for efficient interaction. Clearly, it puts a limit on the cavity separation length L.

Now let us consider another physical effect that limits the bunching in the drift region, namely the self electrostatic field there. As we have seen, the charge density in the interaction region can become infinite when particle overtaking occurs. Clearly this large density will set up a large electric field which will blow appart this space charge accumulation. To look at the effect of the electrostatics, let us consider the beam to be a one dimensional fluid with velocity v_{z0}. The linearized fluid equations of perturbations of density, velocity and z component of electrostatic field are:

$$-\omega n + k n_0 v_z + k n v_{z0} = 0 \qquad (9)$$

$$-i(\omega - k v_{z0}) v_z = -eE_z/m\gamma^3 \qquad (10)$$

$$ikE_z = -4\pi en \qquad (11)$$

where we have assumed perturbed quantities are proportional to $\exp i(kz - \omega t)$. Equations can be reduced easily to the dispersion relation

$$\omega - k v_z = \pm \omega_p \qquad (12)$$

where $\omega_p = 4\pi n_0 e^2/m$. Equation (12) shows that there are two electrostatic modes of oscillation corresponding to the plus or minus sign there. One has a phase velocity faster than the beam, the plus sign, and is called the fast space charge wave. The other has a phase velocity slower than the beam and is called the slow space charge wave. Each one has a group

velocity equal to the beam velocity. If the velocity perturbation is v_z, then Equation (9) shows that the density pertrubation is given by

$$n = -kn_0v_z/(\omega-kv_{z0}) \qquad (13)$$

Now let us consider the beam as it emerges from the first bunching cavity. It has a velocity perturbation denoted by δv_z at frequency ω as it emerges form the cavity, but there is no density perturbation. The velocity and density perturbation must be a linear combination of the fast and slow space charge wave on the beam. By initializing these waves at z=0, we can follow the behavior at other z. The result for the density perturbation is

$$n = -2kn_o\delta v_z/\omega_p\{\sin(\omega[t-z/v_{z0}])\sin\omega_p z/v_{z0}\} \qquad (14)$$

We see that the maximum density perturbation (bunching) is given by $n_0k\delta v_z/\omega_p$ and that this bunching occurs in a distance $\pi v_{z0}/2\omega_p$. Thus for small δv_z the bunching is reduced, but the distance for maximum bunching is also reduced. For the case where the bunching is limited by either thermal spread or electrostatics, the ultimate bunching can be enhanced with additional cavities.

Let us continue with a discussion of the amplification from one cavity to another. Our basic assumption is that fields in a cavity produce only velocity modulation, but no current in that cavity. The current is produced by the ballistic bunching in the drift region between the cavities. As long as there is large amplification from one cavity to the next, the beam loses memory of what happens in earlier cavities because its dynamics is dominated by most recent cavity which had the largest field. Therefore we will discuss a calculation of the amplification from one cavity to the next. To get the total amplification, one simply multiplies the amplification from one cavity to the next by the total number of amplifying cavities.

We assume the cavity operates in the TM_{01} mode, so that the it is characterized by the z component of the electric field. Imagine the n-1st cavity has a field E_{n-1} which gives rise to a velocity modulation in the n-1st cavity. By the time the beam gets to the next cavity, the nth, this velocity modulation gives rise to a current density modulation J_n where the current density is assumed to be in the z direction. This current density might be limited either by thermal or by electrostatic effects. Let us calculate the field that is generated in the nth cavity by this current.

Maxwell's Equation for $E_n(\mathbf{r},\omega)$ is

$$c^2\nabla^2 E_n + i(\omega\omega_0/Q)E_n + \omega^2E_n = 4\pi i\omega J_n \qquad (15)$$

In Eq.(15), the spatial structure is assumed to be nearly a TM_{01} mode, $E_n = E_{0n}J_0(\omega_0 r/c)$ where at the wall, r=a, $J_0(\omega_0 a/c)=0$.Multiplying Eq.(15) by $J_0(\omega_0 r/c)$ and integrating over the volume of the cavity, we find

$$[\omega^2 + i(\omega\omega_0/Q) - \omega_0^2]\, E_{0n} = \{\pi a^2 d[J_0'(\omega_0 a/c)]^2\}^{-1} X$$

$$\int r dr d\theta dz\, 4\pi\omega J_n J_0(\omega_0 r/c) \qquad (16)$$

To write Eq.(16) in the above form, we have made use of the normalization integrals for the Bessel functions. If the current is all localized on the axis of the cavity, the transverse integral can be done and the current density becomes the current. The field in the n^{th} cavity is maximum if it is driven on resonance. In this case the electric field is 90^0 out of phase with the driving current. Far off resonance E_{0n} is smaller and is in phase with the current if driven above the resonant frequency and is 180^0 out of phase with the current if it is driven below the resonant frequency. In designing a klystron amplifier, one makes the tradeoff between amplification ant bandwidth (also equivalent to response time). If one wants large bandwidth and quick response, the cavities would have small Q. On the other hand if one is only interested in maximum amplification from one cavity to the next, one would use a high Q cavity.

Equation (16) is then an expression for the field in the n^{th} cavity driven by the current there. The current is calculated from the fields in the $n\text{-}1^{st}$ cavity by the methods we have discussed earlier in this section. The current might be limited by either thermal or electrostatic effects.. From the fields in the n^{th} cavity, the current can be calculated in the $n+1^{st}$ cavity and the entire process can be iterated. Specifically if the field in the $n\text{-}1^{st}$ cavity is known, the field in the n^{th} cavity can be calculated. The field ratio from cavity to cavity is the amplification factor.

After this brief discussion of the theory of a klystron, let us turn to a discussion of the capability of SLAC klystrons[14]. A photograph of a SLAC klystron, provided by SLAC, is shown in Fig.(1). The three cabinets in Fig 1B hold the modulator which powers the tube. As mentioned, there are seven cavities total. Unlike the HPM sources we discuss in the rest of the paper, the SLAC klystron is driven by a conventional modulator coupled with a pulse transformer to achieve higher Voltage and the beam is produced by a thermionic electron gun. Both the modulator and gun have high average power capability and this is a capability that the HPM sources do not yet have. Typically conventional modulator technology would be applicable up to Voltages in the range of 0.75-1MeV and up to currents of a kiloamp. Thus the maximum beam power in such a system is a gigawatt or less. A thermionic electron source is generally capable of about 10 Amps per square centimeter if long life is required. Thus maximum

cathode sizes of about 100 cm^2 would br required for a kiloamp of beam. Thermionic guns typically require very high vacuum, 10^{-7} Torr or better to operate and the materials that can be used inside the vacuum envelope are quite limited by the necessity to avoid poisoning the cathode. To get such microwave sources to operate at high power generally takes quite heroic measures with the inner surfaces (days of conditioning in various ovens). However once the tube is sealed off, the lifetime is quite long, typically tens of thousands of hours.

The SLAC klystron operates at a frequency of 2.85 GHz. The beam is produced by the thermionic cathode and is focused magnetically and guided by the magnetic field through the interaction cavities. The power is taken out of the last cavity through a radial extraction window. A plot of the amplification, power and efficiency of the SLAC klystron, from Ref 14, is shown in Fig.(2). For a 3.5 microsecond pulse, the power is 67 MW, corresponding to a pulse energy of nearly 250 Joules. Typically, one of the most severe constraints of a SLAC klystron is the necessity to avoid rf breakdown at the output gap. The power of the SLAC klystron can be multiplied at some cost in pulse energy with the SLED pulse compression scheme. Here, the microwave power, after the output is fed into a high Q cavity and switched so as to compress the pulse. Typically the 3.5 μsec pulse is compressed to about 800 nsec with about 60% efficiency.

The development of 2.8 GHz klystrons continues at SLAC. A recent improvement, developed by Lee et al[15] has achieved a power of 150 MW in a 1 μsec pulse at an efficiency of over 50%. This was achieved by both a different klystron configuration and also by operating at higher Voltage. The maximum power was obtained at a Voltage of 475kV. In Ref.(15), it is claimed that this technology can be extrapolated to a power of 700 MW in a 1 μsec pulse. Thus the SLAC klystron, produced by techniques of the conventional microwave tube industry have peak power somewhat less than what we will see the Defense Department laboratories have achieved. However pulse energy is comparable and the average power capability is much greater.

3. INTENSE PULSED ELECTRON BEAMS

Before discussing the different HPM sources developed in the Defense Department Laboratories (as well as Livermore, Los Alamos and Sandia for Defense Department Applications), we will briefly discuss here the technology on which they are based. For at least the last 30 years, the Defense Department has been supporting the development of pulsed power machines. These typically have Voltages of hundreds of kilovolts to megavolts and currents of kiloamps to over one hundred kiloamps. The pulse time however is quite short; fifty nanoseconds is the nominal value, although more and more, these pulse times are being extended to several hundred nanoseconds. These pulsed power machines are typically made for laboratory simulation of charged particle and radiation spectra of nuclear explosions.

Early on, it was realized that the electron beams generated by these pulsed drivers could be used to generate microwaves. Usually these pulsed power machines are quite large. In Fig.(3) is shown NRL's new relativistic klystron facility designed to generate 30 GWs of RF power at 1.3 GHz. This produces a Voltage of typically 1 MeV, a current of 100 kA and a pulse time of 200 nsec. The microwave tube is the main part seen. The power will come out of a horn partially visible on the left. The microwave tube hooks up to the pulse forming line shown to its right. The capacitors which power it are above and to the left. The capacitors which power the magnet needed to confine the beam are not shown in the picture. As is apparent from the figure, the accelerator is quite large. Modern high energy density capacitors can significantly reduce the size of the energy storage element. By using solid state technology, the accelerator can be made more compact, but usually at some sacrifice in rise time or pulse quality. The NRL febetron accelerator is shown in Fig.(4) and a voltage, diode current, microwave tube current, and microwave signal when it runs as a gyrotron are shown in Fig.(5)[8]. While these accelerators can produce high power, they so far have no real average power capability. Typically they are fired once every few minutes. There does not seem to be any fundamental limitation on reprate, however to run at high reprate, all sorts of average power, cooling and thermal management would have to be included and this would complicate the design.

Now let us consider the electron beam production mechanism used with these accelerators. With Voltages of hundreds of kilovolts and gaps of centimeters, almost any surface will field emit. The emission typically takes place by small whiskers forming at the cathode and then explosive

ionization. After the first few nanoseconds, the electron emission is from a plasma produced at the cathode. Typically the cathode material is either graphite or velvet. In some cases, one can use focusing electrodes by using as the electron source a material that emits easily (graphite or velvet for instance) and for the focusing electrode, a material with good Voltage holdoff properties, typically anodized aluminium or polished stainless steel. So far, focusing electrodes have only held off for short times and at relatively low field strengths, but within these constraints have produced very high quality beams[16].

Another difficult with microwave sources powered in such a way is that unlike with a thermionic cathode, the cathode plasma expands after it is produced. The expansion velocity is usually greater than one centimeter per microsecond. Thus if gap spaces are a centimeter of two, the maximum pulse length before gap closure is a microsecond, and the time before the beam characteristics change appreciable is perhaps 100-200 nanoseconds. So far this has proven to be an inherent limit on the system. Enhanced performance would require an advanced cathode which as not yet been developed. Furthermore, once the plasma is produced, it generally takes some time to clear away, perhaps 100 microseconds to several milliseconds. This puts an inherent limit on the reprate of such a system. Furthermore, since the electron emission is from plasma formation, the cathodes generally do not last very long. Their lifetime depends on their ruggedness and the beam power. Usually the cathodes do well to last several thousand shots. At the reprate used in SLAC (180 Hz), this would be less than a minute.

On the other hand, an advantage of such cathodes is that the vacuum requirements are modest compared to thermionic sources; usually 10^{-4} - 10^{-3} Torr is sufficient for good operation. Furthermore virtually any material can be used in the vacuum since there is no surface to poison and the vacuum requirements are much less stringent. Thus these systems are much cheaper to build, take apart, and put back together than the analogous thermionic systems. They can be excellent research tools and with them one can develop changeable, adaptable experimental models of potential thermionic systems. For them to develop into usable systems themselves, one would have to use either a thermionic electron source, which would mean a very large cathode and large area compression (also bringing back all of the vacuum and material constraints) or else develop some sort of advanced cathode with high current density and long life. Also one would have to use a pulse power accelerator with high reprate and average power, which is mostly a technical development project, with no apparent scientific show stoppers.

4. THE RELATIVISTIC KLYSTRON

Since we have begun be discussing the characteristics of the SLAC klystron, it is only natural that we begin our discussion of intense pulsed beam driven HPM sources with a discussion of the relativistic klystron. There are two relativistic klystron projects ongoing now. First there is the SLAC, Livermore, Lawrence Berkeley Laboratory collaboration which is attempting to push conventional klystron technology to higher Voltage, current, and frequency[14,17]. Second there is an NRL effort which is attempting to push to much higher power, but at low frequency[18-20].

We begin with a discussion of the former. Here a thermionic electron gun was used to produce a 1kA beam. The cathode diameter was 12.5 cm and the final beam diameter was less than a centimeter so that large area convergence was used. The electron gun was powered with the Lawrence Livermore Laboratory induction linac, capable of producing 1.3 MeV pulses at a kiloamp. The pulse duration is 40 nsec. Typically the operating current was closer to 500 Amps. This klystron typically had six cavities and a schematic of it , from Ref.14 is shown in Fig.(6). It was designed for efficient operation at a frequency of 11.4 GHz at a power level of 200-300 MW. Because the bunching was dominated by the space charge fields on the beam, the cavities were placed one quarter of a space charge wavelength appart as designated in Eq.(14). The maximum power generated by the relativistic klystron is 290MW at an efficiency of 40%.

Initial experiments on the X-band relativistic klystron showed power of over 200 MW at an efficiency of 32%. The problem was not the power or efficiency, but the pulse shortening[14]. While the electron beam pulse lasted for 40 nsec, the rf pulse typically lasted only for 10 to 20 nsec. Further work identified this pulse shortening as due to large rf electric fields in the output structure which produce secondary electrons which avalanche, generate a plasma and terminate the rf. This difficulty was solved by using a much longer length output structure, a traveling wave structure[17]. Since the electric field in the output structure is proportional to one over the length of the structure, the output field is reduced and the rf pulse lasted as long as the beam pulse. This then summarizes what has been accomplished by the relativistic X-band klystron project.

A very different approach to the relativistic klystron has evolved at the Naval Research Laboratories over the last 5 years. Here the idea is to take advantage of the intense self fields of the electron beam. This is done in two ways, first of all the self fields can enhance the bunching process by operating at a current which is not too far from the limiting current.

Secondly, the self fields of the beam are such that they provide a repulsive force for electrons at the surface of the gaps. This greatly reduces the tendency of rf induced flashover at the output coupling.

Let us look at each of these in turn. To start, we introduce the concept of limiting current. The idea here is that as the beam current increases, the beam has more and more difficulty propagating over its own self potential barrier and ultimately there is a maximum current which can propagate. We will present here one simple calculation of the current limit. Imagine an annular beam of radius r_b traveling down a cylindrical tube of wall radius r_w. At the entrance to the cylinder, that is at z=0, the beam crosses a grounded anode screen and has a relativistic gamma value of γ_i as shown in Fig.(7A). The outer wall of the cylinder is also assumed to be grounded. In the cylinder, far from the screen, the electrostatic potential depends only on radius, and the grounded plane at z=0 has no effect. The next step is to calculate the electrostatic potential between the beam and conducting wall. Using the fact that the current I is related to the surface charge density σ by $I= 2\pi\sigma r_b c\beta$ where $\beta=v/c$, we can integrate the electric field from the beam edge to the cylinder to get the potential drop. This potential drop must reduce the beam kinetic energy. By conservation of energy, we have a relation between the beam energy, current and injection energy. It is

$$\gamma = \gamma_i - I/I_s\beta \qquad (17)$$

where $I_s = 0.5mc^3/e\ln(r_w/r_b)$. (The quantity $mc^3/e = 1.67\times10^4$ Amps and is a measure of limiting currents). Equation (17) above is an implicit equation for γ since γ appears on the left and also on the right through its dependence on β. It is clear however that the beam self fields reduce the beam energy. A plot of electrostatic potential as a function of distance down the guide at the beam radius is shown in Fig.(7B). Notice also that the reduction in beam energy depends on the radius of the beam compared to the cylindrical wall. If the cylindrical wall expands, there is a retarding force on the beam. On the other hand, if the wall converges toward the beam, there is an accelerating force on the beam. For a given wall radius, as the beam current increases, ultimately the energy is reduced so much that the beam cannot overcome its own space charge potential. This gives rise to the concept of a current limit, the maximum current that a beam of energy γ can have.

If Eq.(17) is solved for I and then I is maximized with respect to γ, we find that the current maximizes for $\gamma^3 = \gamma_i$. Inserting this in the expression for current, we find that the maximum current that can be propagated is given by

$$I_m = I_s(\gamma_i^{2/3} - 1)^{3/2} \qquad (18)$$

This then is the maximum current that can be propagated for a beam with an injected energy specified by γ_i. As we will now show, if the current is near the maximum current, a relatively small oscillating field in a cavity can give rise to nearly complete, beam bunching even in the absence of a drift length. To show this, imagine now that at the entrance to the bunching cavity, the beam has energy γ. Across the cavity gap there is an oscillating field giving rise to an oscillation in gamma of $\delta\gamma\sin\omega t$. For half of the cycle of oscillation, the beam speeds up, but for half it slows down. For the half that it slows down, the maximum current is reduced. Indeed, in the expression for the limiting current, Eq.(18), we can obtain the maximum current at the particular $\delta\gamma$ in terms of the maximum current at γ_i by using the fact that in the presence of the oscillating field

$$\gamma_i = \gamma + I/I_s\beta + \delta\gamma\sin\omega t \qquad (19)$$

and solving for the new limiting current. From this limiting current, we can get the maximum retarding voltage at which the beam can propagate across the gap. The result is

$$\delta\gamma_{max} = \gamma_i - [1 + (I/I_s)^{2/3}]^{3/2} = \gamma_i - [1 + (I/I_m)^{2/3}(\gamma_i^{2/3}-1)]^{3/2} \quad (20)$$

Thus at a particular current, there is a maximum retarding potential for which the beam can propagate across the gap. If the oscillating field across the gap is large enough and the current is near enough to the current maximum, that is if $\delta\gamma > \delta\gamma_{max}$, the beam may be stopped for a portion of the rf cycle. As long as this is so, the phase of the stopped region is given by

$$\Phi = \pi - 2 \arcsin \delta\gamma_{max}/\delta\gamma \qquad (21)$$

Of course on the average, the beam current is less than the maximum current, so in the accelerating phase of the Voltage waveform, all the beam gets through. If we make the simplest assumption, namely that the portion of the beam which is stopped is uniformly added on to the passing portion, we find that the current of the modulated beam divided by the average current is given by

$$I_m/I = 2/[1 + (2/\pi) \arcsin\delta\gamma_{max}/\delta\gamma] \qquad (22)$$

For large modulating field (large $\delta\gamma$), the current modulation is 2, corresponding to the stopped half of the beam adding to the transiting half

in the transiting half cycle. If $\delta\gamma$ is just slightly larger than $\delta\gamma_{max}$, the onset of bunching is very sudden, with the additional density proportional to $[1-(\delta\gamma_{max}/\delta\gamma)]^{1/2}$. Thus the strong self fields of the beam can significantly enhance the bunching of the beam, and do so without even the use of ballistic bunching.

We will now discuss another way in which the strong self fields can enhance the bunching. Recall that if the guide radius increases, the maximum current decreases, corresponding to a retarding potential. On the other hand, if the guide radius increases, the maximum current increases, corresponding to an accelerating potential. As the beam passes by the bunching cavity, it first sees a larger wall radius and then sees the wall radius go back to its initial value after it has passed by the cavity. Thus, as the beam passes by each cavity, it sees a potential barrier which is caused by its own space charge. Let us examine the effect of this potential barrier on beam bunching. If two particles are separated by a distance d, and the front one travels at speed v_1, and the rear one travels at a greater speed v_2, the latter catches up to the former in a distance $d/(v_1-v_2)$. Now consider the situation if there is a potential barrier, of height ϕ and distance L that each particle must cross before the faster catches up to the slower.

To simplify this calculation, we will assume that this potential is small so that the unperturbed orbits are a good approximation to the motion. Furthermore, after making the initial assumption of unperturbed orbits, we will approximate the spatial profile of the potential with a delta function, $\phi(x) = \phi L\delta(x-x_0)$. If the forward particle starts at x=0 and the rear starts at x=-d at time t=0, then the orbits of the particle after each has crossed the barrier are

$$x_1(t) = v_1t - e\phi L/m\gamma_1^3v_1^2 \qquad (23)$$

and

$$x_2(t) = -d + v_2t - e\phi L/m\gamma_2^3v_2^2 \qquad (24)$$

The bunching distance is reduced by $(e\phi L/m)[\gamma_1^{-3}v_1^{-2} - \gamma_2^{-3}v_2^{-2}]$. This is illustrated in Fig.(8). Thus we see that the strong self fields of the beam enhance the bunching in two significant ways, first they give rise to direct bunching as the beam is turned around by the fields in one of the cavities; and second, they give rise to a shortened bunching distance as the beam overcomes its only self potential at the bunching cavity. This appears to be

the reason that the NRL relativistic klystron experiment does not need many cavities or a long bunching length.

The self fields of the cavity also have another important effect on the operation of the NRL device. As we have seen, in both the SLAC klystron and the SLAC-LLNL-BNL relativistic klystron, one of the greatest constraints is the rf induced breakdown at the output gap. The NRL relativistic klystron appears to operate free of this difficulty and the reason seems to have to do with the beam self fields once again. If there were no beam self fields, the rf field would tend to pull electrons off of one side of the gap during one half of the rf cycle and off of the other side during the other half. At one half of the cycle, the potential (that is the negative integral of the rf electric field) across the gap would depend on distance as shown in for instance Fig.(9A). With this polarity, electrons would tend to be emitted from the left side, but would not be emitted from the right. Note however that the self fields of the beam tend to repel other electrons, so that they add an additional potential barrier for the electrons on the left side of the gap. That is, in the presence of the beam self field, the total potential is as shown in Fig.(9B). Notice that the field now has the sign to drive electrons into the wall at *both* sides. In Fig (10), from Ref .20 is shown a computer plot of the electrostatic potential in the gap and the drift tube for a configuration of the NRL experiment. Notice that the equipotential contour, as generated by the beam self field, bulges into the cavity with such polarity as to force the electrons into the wall on both sides.

Now let us review the experimental results achieved on the NRL relativistic klystron. A configuration of the device is shown in Fig.(11). This figure is reversed from the usual in that the beam propagates from right to left. The beam Voltage is typically 500kV and the current is about 10 kA. About 100 kW of rf power at 1.3 GHz is injected into the first cavity from a magnetron. This modulates the velocity of the beam. The beam ballistically bunches and enters the second cavity where it is bunched further. Notice that only two cavities are necessary for full bunching even though the beam has a γ of about 2 and is therefore quite stiff. This contrasts to the six or seven cavities needed in a conventional klystron. The output is taken to the left of the second cavity. Shown in the figure is the beam collector. After the second cavity, the beam is fully bunched and hits the collector. Before it hits the collector, it travels across an rf gap where the beam loses its energy to an oscillating rf field. The rf gap is connected to a coaxial transmission line and as the beam propagates down the line, the center conductor tapers down and radiation transitions to fundamental waveguide mode and is extracted into the atmosphere. A plot

of the beam power as a function of time, form Ref 20 is shown in Fig.(12). The efficiency is over 30%. The maximum power exceeds two gigawatts and the rf energy in the pulse is about 200 Joules. Thus, as compared to a SLAC klystron, the power is much higher, but the energy per pulse is comparable. Efforts are now underway at NRL to increase the pulse energy to over one kilojoule.

5. INTENSE BEAM DRIVEN MAGNETRON

The magnetron is one of the oldest of the microwave tubes still in use. The cavity magnetron was of course what played such a vital role in the the development of radar in the Battle if Britain in World War II. It is still one of the most successful intense pulsed beam driven HPM sources. It is also one of the most efficient conventional microwave tubes. The microwave oven magnetron, at 2.45 GHz can be as much as 80% efficient. The magnetron is not as well understood as other devices, in large part because of the complex geometry and the cross field nature of the interaction. Excellent reviews of the theory of intense beam driven magnetron theory and experiment have been given by Lau[21], Benford[22], and Miller[23]. We will discuss first the free running oscillator magnetron, and then discuss some recent experiments on phase locking magnetrons at high power. As we have done so far, we begin with an outline of the theory of the device.

A. Free Running Magnetron Oscillators.

The two dimensional configuration of the magnetron is shown in Fig(13A). In Fig (13B) is shown a planar version where the spatial dimensions are also shown. There is a dc electric field between the smooth inner conductor and the outer conductor. The outer conductor is not smooth, but has resonant cavities in the wall as shown. The case shown, Fig.(13A) is taken to have six equivalent cavities. Other configurations are possible including unequal cavities and even cavities on the inside. In the configuration shown, the inner conductor is the cathode. In addition, there is a magnetic field perpendicular to the plane of the paper. Because of the magnetic field, the electrons cannot be accelerated directly across the gap to the anode. Instead, they ExB drift around the the azimuthal direction as long as the electric and magnetic field are within certain broad limits. Virtually all theory considers the two dimensional nature of the interaction and does not consider the complications of the top and bottom wall which have to be present to limit the interaction in the axial direction. Now let us consider waves in the device. Consider for a moment the smooth wall version in planar geometry. This is transmission line supporting TEM modes with the dispersion relation $\omega = ck$. Also it is a waveguide supporting TE and TM modes with dispersion relation $\omega^2 = c^2k^2 + \omega_c^2$, where ω_c is the cutoff frequency for the particular mode in the wave guide. Since the phase speed is equal to the speed of light for the former, and greater for the latter, it is clear that the wave cannot resonate with the

particle motion. The role of the cavities in the outer wall is to slow down the azimuthal phase speed of the wave in such a way that it is equal to the particle speed so that there can be efficient wave particle energy transfer.

These then are the elements of the theory of the magnetron which we will discuss, the range in voltage and magnetic field where electrons orbit around the cathode, the role of the cavities in slowing down the azimuthal phase velocity in the cavity, and the range of voltage and current where the phase velocity is equal to or less than the maximum electron drift speed. In addition, we will discuss in a qualitative way the elements of the nonlinear theory, which indicate why the magnetron has such a high inherent efficiency.

We start with the condition for azimuthally orbiting electrons, also called the condition for magnetic insulation, and also called the Hull cutoff. Throughout, we will consider the planar model of Fig (13B). To simplify the matter further, when we calculate the condition for magnetic insulation, we consider the configuration where both walls are smooth. The condition for magnetically insulated flow is determined simply by two conditions. The first is energy conservation,

$$(\gamma-1)mc^2 - e\phi = 0 \qquad (25)$$

where ϕ is the electrostatic potential between the cathode and anode and it is assumed to be zero at the cathode. If x is the coordinate between the cathode and anode, and is zero on the cathode, the second condition is that the velocity is the ExB drift velocity

$$v = (c/B)\, d\phi/dx \qquad (26)$$

The relation between γ and v is $\gamma = [1 - v^2/c^2]^{-1/2}$. Differentiating Eq.(25) and combining with Eq.(26), it is not difficult to solve for v as a function of x and find

$$v = c \arcsin\{(\Omega_c x/c)[1 + (\Omega_c x/c)^2]^{-1/2}\} \qquad (27)$$

where $\Omega_c = eB/mc$. From the equation for v, it is a simple matter to solve for ϕ as a function of x. The result is

$$\phi = (mc^2/2e) \ln[1 + (\Omega_c x/c)^2] \qquad (28)$$

From the voltage in Eq.(28), we can find the expression for the space charge density from Poisson's equation. It is simple to see that at the cathode, the plasma frequency and electron cyclotron frequency (nonrelativistic version of each) are related by

$$\omega_{pe}^2 = 2\Omega_{ce}^2 \qquad (29)$$

Equation (28) for the potential is only valid in the region where the space charge exists. Fundamental to the operation of the magnetron is the fact that the space charge cannot reach all the way up to the anode, or the device will be short circuited. Above the space charge layer, the electric field in constant as a function of x. Assuming that the voltage across the plates is V, the gap width D and the magnetic field B, one can determine the condition for magnetic insulation. To do so, first determine the electric field at the top of the layer, at y=H by differentiating Eq.(28). Above this point the electric field is constant and the voltage increases linearly in x-H. The Voltage at the edge of the space charge layer is given by Eq.(28) at x=H. This lets us relate V, H, D and B. If the voltage is too high, the relation cannot be satisfied for H<D. Setting H=D gives a relation for the maximum Voltage at which magnetic insulation can be maintained. This is

$$V = (mc^2/2e)\ \ln[1 + (\Omega_c D/c)^2] \qquad (30)$$

This maximum voltage is also called the Hull cutoff. It is the upper curve shown in Fig.(14).

There is also a minimum voltage necessary for oscillation given by the fact that the maximum ExB drift velocity of the electron, the drift velocity at the edge of the space charge layer be greater than the phase velocity of the wave. This gives a minimum Voltage which is dependent on the wave phase velocity, and therefore on the details to the shape of the anode. Plotting this condition schematically, it is the lower curve in Fig (14). It is called the Hartree Buneman oscillation threshold. The region of operation of a magnetron is then the Voltage range between the Hartree oscillation threshold and the Hull cutoff. It is shown as the shaded region in Fig.(14).

Now let us examine the dispersion relation of the wave in the planar version of the magnetron, Fig (13B). This comes to a solution of Maxwell's equations in a periodic configuration. By Floquet's theorm, we know that the eigenfunction is given by expiky times a function which is periodic in y with period d. That is the eigenfunction which in this case will be assumed to be the z component of magnetic field (corresponding to TEM or TE polarization) has the spatial dependence given by

$$B_z(x,y,t) = \quad B_n(x)\exp(iky - i\omega t + 2\pi i n y/d) \qquad (31)$$

The dispersion relation is the relation between ω and k. We will consider a transmission line mode modified by the periodic structure, because that is

the simplest dispersion relation to derive, and also it is the mode whose phase velocity is easiest to slow down to less than the speed of light. Just by virtue of the nature of the periodic structure, it is a simple matter to see that there are wave whose phase velocity is slow, and in the case of a transmission line, go to zero. To see this note that from the form of the eigenfunction given in Eq.(31), it is clear that nothing changes if k increases by $2\pi n/d$. Thus, ω must be a periodic function of k with this periodicity. In the smooth walled system, there are unique values of ω which for arbitrary values of k. Thus in the periodic walled system, these must split into different branches of a more complex dispersion relation. In Fig (15A) is shown several of the branches of the dispersion relation for the TEM mode of the periodic system, with the smooth walled dispersion relation shown as the dotted curve. In Fig (15B) is shown the analogous thing for a waveguide mode. Clearly by the periodic nature of the dispersion relation, there are modes which have small phase velocity for the waveguide case, and modes which have zero phase velocity for the transmission line case. In each case, there are modes with negative group velocity also.

We now get the dispersion relation for the transmission line mode in the presence of the cavities in the wall. First look at the straight sections of the line. The electric and magnetic fields here is given by

$$E_x = E_0 \exp i(k_0 y - \omega t) \qquad (32a)$$

$$B_z = E_x \qquad (32b)$$

where $k_0 = \omega/c$, the value determined by the transmission line dispersion relation. Notice that the field in the straight section is a linear combination of a wave going in the positive and negative direction and the relative coefficients are unknown at this time. To relate this most easily to transmission line theory, we can define a voltage drop across the guide as $V = -ED$ and a current in the guide as $I = cBL/4\pi$ where L is the width of the guide in direction transverse to the paper. This allows us to define a guide impedance as $\eta =$
$V/I = 4\pi D/Lc$. Imagine that at y=0, just to the left of the transverse stub cavity, the voltage and current are given by V_0 and I_0. This allows us to solve for the electric field coefficients of the forward and backward propagating waves as

$$E_{0+} = -V_0/2D + 2\pi I_0/Lc \qquad (33a)$$

$$E_{0-} = -V_0/2D - 2\pi I_0/Lc \qquad (33b)$$

This then allows us to get the Voltage at y=d-s (Actually s is assumed small compared with both d and c/ω so that we can assume this is the value of voltage and current at y=d as long as it is understood that this means in front of the stub cavity.) The current at this point can be calculated in terms of the Voltage by using the impedance of the smooth section of the transmission line.

Now consider the stub. If x=0 is taken at the top of the stub, at the bounding conducting wall, then the electric and magnetic field in the stub is given by

$$E_y = E_s \sin k_0 x \exp -i\omega t \qquad (34a)$$

$$B_z = -iE_s \cos k_0 x \exp -i\omega t \qquad (34b)$$

Calculating the Voltage across the stub and the current down it as before, we find a stub impedance given by

$$\eta_s = (4\pi i s/cL) \tan k_0 x \qquad (35)$$

The current down the stub at the position where it meets the flat section of the transmission line must equal to the current at that point in the transmission line. From the stub impedance, we can then get the Voltage across the stub at the opening. This then allows us to calculate the voltage V_1 and current I_1 just across the stub in terms of V_0 and I_0. In matrix form, this can be expressed as:

$$\begin{matrix} V_1 \\ I_1 \end{matrix} = \mathbf{M} \begin{matrix} V_0 \\ I_0 \end{matrix} = \exp ikd \begin{matrix} V_0 \\ I_0 \end{matrix} \qquad (36)$$

where the last equality comes from Floquet's theorm. When the elements of the matrix are inserted, we find that the dispersion relation is

$$2\cos kd - 2\cos k_0 d + \{cLs/4\pi D\} \sin k_0 d \tan k_0 g = 0 \qquad (37)$$

This is to be solved for the frequency ω, which is $k_0 c$, in terms of k. To derive this dispersion relationship as simply as we did, we relied on the fact that only transmission line modes were present in both the the smooth walled section and the stub. This means that the wavelength of the modes in question must be long compared to such dimensions as D and s. If this

condition is violated, waveguide modes can also impact the properties of the electromagnetic field in the resonator and the derivation of the dispersion relation becomes much more complicated.

We have seen that the periodic structure in a parallel plate configuration has an important impact on the frequencies of the modes. However the values of k are a continuum. In a magnetron, however, the system closes on itself. In the planar model of the closed magnetron configuration, k can only take on those discreet values which impose an overall periodicity in the solution. For the magnetron configuration shown in Fig.(13A), there are six cavities around the circumference. This is called the A-6 magnetron. Thus the phase shift between cavities cannot be arbitrary, but must be an integral times $\pi/3$. The dispersion relation of the magnetron shown in Fig.(13A) is displayed in Fig (16). The mode of the magnetron is usually denoted by the phase shift between adjacent cavities. As can be seen from Fig. (16), the π mode on the lower branch happens to have the same phase velocity as the 2π mode on the upper branch. This can make it difficult to predict which mode the magnetron will oscillate in. Generally it is thought that best operation is in the π mode.

Let us look more carefully at the interaction in the magnetron. To start note that since the wave travels slower than the speed of light in the y (or θ) direction, it is evanescent in the x (or r) direction. Since the anode surface is the irregular one, the wave amplitude maximizes near the anode and then decreases as one approaches the cathode. In Fig.(17) is shown the planar version of the magnetron where now the electric field lines are shown at a particular time. The magnetron operates in the π mode in Fig.(17), and the entire field pattern moves to the left with the phase velocity. The electron also moves to the left with the ExB velocity. Consider the electron labeled A Since the electric field and particle velocity are in the same direction, this particular electron loses energy. However as it loses energy, its ExB drift velocity from the rf electric field is upwards toward the anode. Thus the drift velocity gets faster and faster because the rf field increases as one approaches the anode. Now consider another electron B which has the rf electric field opposed to v so that it gains energy. Its drift velocity is downward toward the cathode. When it reaches either the cathode or the main part of the magnetically insulated cloud, it regains potential energy. At a later time can start again and reenter the gap and this time perhaps lose its energy. Thus if the electron has such a phase as to lose energy, it makes it up to the anode and is lost. If it has such a phase as to gain energy, it goes back to the cathode or magnetically insulated charge cloud and can try again later. The electron loses its energy via the work done by the rf electric field against the ExB drift. However this ExB drift is not itself an energy source, but more of a

catalyst; it allows the rf field to do work against the loss of potential energy the electron undergoes when it falls from the cathode to the anode.

Another aspect of the magnetron that promotes its good performance is the principle of phase stability. Imagine that electron A has phase speed slightly greater than the phase speed of the wave. Then it will get ahead of the wave and get to point P where the field is vertical. The ExB drift velocity from the rf field at this point is to the right, so that the electron drifts back to the point where its energy loss is maximized. Now consider the electron B which gains energy from the wave. It drifts ahead to point Q. However at this point the drift ExB drift velocity with the rf field is to the left, so the electron tends to get further out of phase with the wave. Thus the electrons which lose energy remain in phase, and those that lose energy get out of phase.

We now investigate further the orbits of particles in the magnetron. To start, we assume a smooth anode surface and further assume that the dc electric field is uniform in x. Thus there is no shear in the ExB drift velocity of the electrons in the y direction. We assume that the phase velocity of the wave is equal to this ExB drift velocity. We do our calculation in the reference frame in which the wave and ExB drift velocity is zero. If the phase speed, and ExB drift speed are nonrelativistic, the electric field is nearly derivable from a potential

$$E = -\phi, \quad \phi = \phi_0 e^{kx}\cos ky$$

Here we assume that x=0 is the cathode surface. The exponential increases from the cathode to anode, rather than visa versa, because the cathode is the smooth surface.

In the drift frame, we can calculate the equation for the orbit by taking the ratio of velocity in the x and y directions. The result is

$$dx/dt = \tan ky \qquad (38)$$

or

$$kx = \ln \sec\{\sec ky/\sec ky_0\} \qquad (39)$$

where y_0 is the position of the particle on the cathode, at x=0. There are solutions for positive x as long as $\pi/k < y_0 < 2\pi/k$, that is as long as the initial ExB drift velocity in the fluctuating field is positive, or in other works, as long as the electron loses energy in the laboratory frame. The shape of the electron boundaries, in the drift frame, appears as shown in Fig.(18). The electrons start over half of the cathode surface, and accelerate upwards and converge on the position at which the actual retarding field maximizes. This has the same general appearance as the

spoke formation in particle simulations of magnetron behavior. In Fig.(19) is shown a phase plot from such a particle simulation, where the formation of the electron spoke is apparent. This picture, reproduced from Ref. 22 originally appeared in the Ph.D thesis of Alan Palevski[25].

The key to the magnetron's high efficiency is that it is one of the only rf sources that converts *potential* energy to radiation. That is, when an electron makes it from the cathode to the anode, it falls through a potential V. However, the kinetic energy of the electron striking the anode is much less than this. The difference is made up in what energy the electron radiates away. Note also that the current depends crucially on the radiation for its existence; without the radiation, the electrons would just exist in the Brillouin layer around the cathode and would not reach the anode. Let us obtain an approximate expression for the current in terms of the rf field ϕ_0. The average ExB drift velocity in the x direction at the cathode is $2ck\phi_0/\pi B$ over the half wavelength portion which emits electrons. The charge density at the cathode, according to Eq.(29) is given by $2m\Omega_c^2/4\pi e^2$. The current is the current density times the area of the emitting surface. Assuming that the length of the magnetron perpendicular to the page is L, that the cathode is a circle of radius R, and that half of the cathode emits current which is collected on the anode, we find that the current is given by

$$I = kRL\phi_0 eB/\pi mc \qquad (40)$$

Next, we will calculate an approximate expression for the efficiency. To do so, we assume that when the electron reaches the anode it has fallen through a potential V and has kinetic energy $(\gamma-1)mc^2$, where γ characterizes the kinetic energy as it strikes the anode. the remaining energy is assumed to be radiated away. Thus the efficiency η is given by

$$\eta = [eV - (\gamma-1)mc^2]/eV. \qquad (41)$$

The remaining thing is to calculate γ. To do so, we assume that the y velocity upon striking the anode is the dc ExB drift (recall that near the anode, the electron is localized in the field near a position where the y component of the ExB drift vanishes). The x component of velocity is given by the ExB drift in the rf field. Making this assumption, we find that when the electron strikes the anode,

$$\gamma = \{1 - [(k\phi_0/B)\exp kd]^2 - [V/dB]^2\}^{-1/2} \qquad (42)$$

The power output of the beam is then

$$P_b = \eta IV$$

As a function of rf electric field ϕ_0, P_b initially increases linearly with ϕ_0 as the current increases with ϕ_0, and then begins to decrease with ϕ_0 as the kinetic energy begins to increase, causing the efficiency to fall off with ϕ_0. A plot of beam power output versus ϕ_0 is shown in Fig.(20). We would like to design the cavity so as to optimize the power of the magnetron. The rf power output is

$$P_{rf} = \zeta \omega k^2 \phi_0^2 R^2 L / 8\pi Q \qquad (43)$$

where ζ is a dimensionless factor. Here Q is the cavity quality factor; the quality factor is assumed to be determined entirely by the output power of the magnetron. For the magnetron to operate in steady state, P_b must be equal to P_{rf}. Designing the cavity for optimum power output then means designing the proper cavity Q. Also shown on Fig (20) are three curves for P_{rf} as a function of ϕ_0, the three parabolas. The heavy solid one has a Q designed for optimum output power. The left hand light curve has too small a Q, so the fields cannot build up to a level which would give rise to optimum power. We call this cavity underdriven, in the sense that the current is too small to drive it to maximum output power. The right hand light curve has too large a Q; the fields are so large that the efficiency begins to fall off so the power is less. We call this cavity overdriven in that the current is too large for optimum operation.

Experiments on intense beam magnetrons have taken place in the United Stated at MIT[24,25] and Physics International Corporation[22,26], as well as at other places[27-30]. Both of these were with six vane magnetrons, what MIT has called the A6 magnetron. A schematic of the A6 is shown in Fig.(13A). There, the power is taken out of a waveguide hooked up to one of the cavities. MIT has achieved power of about 900 MW at a frequency of 4.6 GHz. The pulse time is typically about 20 nsec, which is less than the diode time of perhaps 40 nsec. As a function of magnetic field, the power has a strong maximum just above the Hartreee Buneman oscillation threshold at about 8 kG. Experiments at Physics International are on a larger generator and operate at higher power. A photograraph of the S-Band magnetron setup at PI, from Ref 22 is shown in Fig.(21). If power is extracted from one vane, it is typically 1.5 GW. By extracting form more than one vane output power can be increased. The output power maximizes at about 3 GW when three vane extraction is used. If more power is taken out of more vanes, the output power begins to drop again, as shown in Fig.(22). This rise and drop then shows the dependence of output power on Q which we have just discussed. The efficiency of the PI magnetron was typically 20%. Thus intense relativistic beam magnetrons

have achieved fairly high efficiency, but not as high as that achieved by low voltage magnetrons. Typically it also achieved best operation near the Hartree Buneman threshold.

B. Phase Locked Magnetrons...

The intense beam magnetrons which we have discussed are free running oscillators. An important question, particularly as regards whether these magnetrons can power accelerators or phased arrays is whether they can be phase locked. This is one of the oldest problems in nonlinear mechanics and dates back to the sixteenth century when Huygens noticed that two clocks hung on the same wall will synchronize one another if there rates are nearly the same. The question is then under what circumstances two magnetrons will synchronize, or phase lock one another. We will start off with a simple nonlinear oscillator model for the coupled magnetrons. To start consider a single magnetron as a nonlinear oscillator. Calling the dependent variable E_1, we assume the equation for the oscillator is

$$d^2E_1/dt^2 + \{(\omega/Q-\gamma) + \beta E_1^2\}dE_1/dt + \omega_1^2E_1 = 0 \qquad (44)$$

Let us assume a solution like $E_0\cos\omega t$. Multiplying Eq.(44) by $\cos\omega t$ and integrating over t from 0 to $2\pi/\omega$, we find that $\omega = \omega_1$. Multiplying by $\sin\omega t$ and integrating over t from 0 to $2\pi/\omega$, we find

$$(\gamma_1 - \omega/Q) = (\beta/2)E_1^2 \qquad (45)$$

Thus Eq.(45) is an equation for the mode amplitude. We have distinguished two contributions to the linear growth term. The first is ω/Q which represents the output of the oscillator and is a damping term. It is what relates power to field. The power of the oscillator is proportional to $\omega E_0^2/Q$. The second, γ represents the instability mechanism, the beam wave interaction in the case of the magnetron. The β term is a nonlinear damping term which is responsible for limiting the amplitude of the wave.

Now let us consider two oscillators with independent variables E_1 and E_2, and at slightly different frequencies, ω_1 and ω_2 and coupled to each other. Other than the slight difference in frequency, the two equations are the same, so the oscillators will have the same amplitude, and nearly the same frequency. As a coupling, we will assume a term on the right hand side of Eq.(44) of αE_2 and a term on the right hand side of the analogous equation for E_2, the coupling term $-\alpha E_1$. The coupling conserves energy between the two oscillators. Now let us consider the condition for the two oscillators to lock one another. To do so, we will

consider the coupling to be weak, so that the amplitudes of the oscillators are unaffected by the coupling.

For the first oscillator, let us assume a solution $E_0\cos\omega t$, and for the second, assume the solution $E_0\cos(\omega t+\phi)$. By taking the in phase portion of the two equations for E_1 and E_2, we will solve for ω, the common frequency and ϕ, the phase shift. Multiplying Eq.(44) by $\cos\omega t$ and integrating over t, we find

$$\omega_1-\omega = (\alpha/2\omega)\cos\phi \qquad (46)$$

Taking the analogous equation for E_2, multiplying by $\cos(\omega t+\phi)$ and integrating over t, we find

$$\omega_2-\omega = -(\alpha/2)\cos\phi \qquad (47)$$

Adding Eqs (46) and (47), we find that the common frequency is the average of the two individual frequencies. Knowing the frequency, Eq.(46) gives an expression for the phase shift ϕ. In order to have a phase locked solution at all, Eq.(46) and the expression for ω shows that the condition
$\omega_1-\omega_2 < \alpha/\omega$ must be satisfied. If it is not, there will be no phase locked state and the two oscillators will affect one another, but they will not be able to synchronize one another.

Now let us see how the oscillators approach the phase locked equilibrium. Inserting $E_2 = E_0\cos(\omega t+\phi)$ into the equation for E_2 and assuming that the phase is a slowly varying function of time and ω is nearly equal to ω_2 we find

$$d\phi/dt = \omega-\omega_2 - (\alpha/\omega)\cos\phi \qquad (48)$$

If there is no time dependence, Eq.(48) above gives the equilibrium condition as expressed in Eq.(47). If ϕ is slightly different from its equilibrium value, the equation for the perturbed value, $\delta\phi$ is given by

$$d\delta\phi/dt = [(\alpha/\omega)\sin\phi_0]\delta\phi \qquad (49)$$

As long as the equilibrium phase ϕ_0 is between π and 2π, the system is stable, and the phase approaches its equilibrium value exponentially with time constant $(\alpha/\omega)\sin\phi_0$.

In order to investigate the phase locking of two magnetrons, an experiment at Physics International Company hooked up two intense beam magnetrons to the same accelerator and connected the two via a waveguide between two of the cavities[31,32]. A plunger in the connector allowed the

coupling to be varied. A schematic of the experiment, from Ref 32 is shown in Fig.(23A). It was found that the phases of the two magnetrons did indeed approach a common value. In Fig.(32B), also taken from Ref 32 is shown the phase difference between the two over 7 shots. Clearly this phase difference approaches a common value, as predicted by the theory of phase locked oscillators. The total power of the two magnetrons together is 2.8 GW, and the frequency is 2.8 GHz in the π mode operation. Thus, it has been demonstrated that phase locking is possible for two separate intense beam powered magnetron oscillators.

6. THE VIRCATOR

One high power microwave source which has been studied a great deal in the defense department community is the virtual cathode oscillator, or vircator. As we have seen in our discussion of the relativistic klystron, as the current of the beam increases, it has a harder and harder time getting over its own potential barrier. Ultimately the current is so great that the beam cannot get over this barrier at all. If the beam is injected into an open propagation region, through a grounded foil for instance, it will propagate for a certain distance and then reflect from its own space charge cloud. This point of reflection is called a virtual cathode.

The reflexing of electrons from the virtual cathode is quite complex and nonlinear in nature. As the individual electrons reflex, they have a frequency associated with the individual electron motion. Furthermore the electron cloud at the virtual cathode can itself oscillate. Both of these frequencies are of order of the electron plasma frequency, $\omega [4\pi ne^2/\gamma^3 m]^{1/2}$, where n is the electron beam density. However the two frequencies are not exactly the same in general. As both the individual electrons and the electron cloud oscillates, it can radiate at one or both of these frequencies. This type of high power microwave source is called a vircator. Since it is inherently a very high current device, the power is typically extremely high. However the efficiency is very low, typically 1% or less. Also, since in the usual configuration the electrons just propagate down a straight pipe, there is nothing to pick out the mode or phase, so vircators a characterized by mode hopping and frequency chirping. This chirping results from the fact that the density increases in time as the diode begins to short out. Thus in general, vircators are characterized by an increasing frequency chirp. Despite their low efficiency and poor pulse quality, vircator are of interest to the defense department because of their high power and simplicity. Virtually nothing is needed except an electron beam source. This power and simplicity makes vircators particularly interesting for single shot or explosively driven microwave generators.

Since vircators are inherently complex and nonlinear, most theoretical work done on them has been through numerical simulation. Experimental work on them has gone on at one time or another at most defense department laboratories. The frequency is typically S-Band or below[33-37], although a vircator experiment at Los Alamos[38], and NRL[39] has generated very high power at 17 and 35 GHz. More typical is the result at Physics International where frequencies of 2-4 GHz are the norm.

In these experiments, the frequency tends to chirp, as we have just discussed. However by inserting the oscillating virtual cathode in a microwave cavity, the frequency can be stabilized. For instance, in Fig.(24A), from Ref 36 is shown the spectrum of the oscillation of the PI vircator without a cavity, and in Fig (24B) the spectrum with a cavity. Clearly the line width decreases by about a factor of three with a cavity.

One of the best improvements of the vircator in the published literature is the Reditron[40,41], developed at Los Alamos. The idea behind the reditron is that one reason for the poor efficiency of the vircator is that the reflexing electron frequency is different from the charge cloud oscillation frequency and the result is a destructive interference which impedes performance. To avoid this, the reditron eliminates the reflexing electrons. It does this by launching the beam into the interaction region through an annular slot in a range thick anode, usually a piece of graphite about a centimeter thick. The electrons which are reflected will in general strike the graphite and be lost. Other electrons will transit through the interaction region. Thus there is only one frequency, the frequency of the oscillating virtual cathode. A schematic of the reditron, from Ref 40 is shown in Fig.(25). In Fig.(26), also from Ref 40 is shown a particle simulation of the reditron, showing that particle either transit the device and strikes the wall by following the magnetic field (which flares outward), or else reflexes once and strikes the anode. This particular device at Los Alamos has achieved a power of 3.3 GW at a frequency of 2.15 GHz. The efficiency of the device was about 10%, corresponding to nearly an order of magnitude increase over previous vircator experiments.

Conclusions

In this memo we have discussed high power microwave sources as developed by both the Department of Defense and Department of Energy. There are areas of commonality, but also significant differences between the routes taken by the two organizations. It is hoped that this review will give rise to a broader understanding of the similarities and differences and thereby enhance the research in both.

Acknowledgment

The author has benefitted from discussions with Y.Y. Lau, Moshe Friedman, Matt Allen, and James Benford. This work was supported by the Office of Naval Research.

REFERENCES

1. W. Eckhardt, J. Small, and F Chilton, "Decoy Discrimination Using Ground-Based High Power Microwaves" Proc. SPIE, Volume 873, p 112, 1988
2. H.K. Florig, "Microwave Battlefields", IEEE Spectrum, March, 1988
3. W.M. Manheimer, High Power Micorwave Directed Energy for Naval Applications", NRL Memorandum Report 6604, 1990
4. A. Kehs et al, IEEE Trans. Plasma Sci. PS-13, 559, (1985)
5. Y. Carmel et al, Phys. Rev. Let. 62, 2389, (1989)
6. J. Nation et al, Proc. SPIE, Vol. 1061, p17, (1989)
7. Bugaev et al, Proc VI Intl Conv on High Power Beams (Beams 86), 1985, p. 584
8. S. Gold et al, Phys. Fluids, 30, 2226, (1978)
9. W.M. Black et al, Phy. Fluids B, 2, 193, (1990)
10. S. Gold et al, Phys. Rev. Let. 52, 1218, (1984)
11. T. Orzechowski et al, Phys. Rev. Let. 57, 2172, (1986)
12. A. DiRienzo. Proc. SPIE, Vol 1061, p 238, (1989)
13. S. Gold et al, Phys. Fluids, 26, 2683, (1983)
14. M. Alle , Invited Presentation, European Particle Accelerator Conference, Rome, Italy, June, 1988
15. T. Lee et al, IEEE Trans. Plasma PS-13, 545, (1985)
16. D. Kirkpatrick, Ph.D Thesis, MIT, January 5, 1988
17. M. Allen et al, Phys. Rev. Let. 63, 2472, (1990)
18. M. Friedman et al, J. Appl. Phys, 64, 3353, (1988)
19. M. Friedman and V. Serlin, IEEE Trans. Electr. Insul. EI-23, 51, (1988)
20. M. Friedman et al, Rev. Sci. Instrum. 61, 171, (1990)
21. Y.Y. Lau, in "High Power Microwave Sources", ed. Granatstein and Alexeff, p 309, Artech House, 1987
22. J. Benford, in "High Power Microwave Sources", ed. Granatstein and Alexeff, p. 351, Artech House, 1987
23. R.B.Miller, "Intense Charged Particle Beams",Plenum Press, 1982 , Chapter 6.1,
24. A. Palevsky and G. Bekefi, Phys. Fluids, 22, 986, (1979)
25. A. Palevsky, Ph.D. Thesis, MIT, June, 1979
26. J. Benford et al, IEEE Trans. Plasma Sci, PS-13, 538, (1985)
27. T. Treado et al, IEEE Trans. Plasma Sci, 16, 237, (1988)
28. W. P. Ballard, S. A. Self and F.W. Crawford, J Appl. Phys, 53, 11, (1982)
29. H. Sze et al, IEEE Trans Plasma Sci. PS-15, 327, (1987)
30. N.F. Kovalov, Sov. Tech Phys. Let. 6, 4, (1980)

31. J. Benford et al, Phys. Rev. Let. 62, 969, (1989)
32. J. Levine et al, Proc. SPIE, Vol. 1061, p.144, (1989)
33. H. Sze et al, IEEE Trans. Plasma Sci. PS-13, 492, (1985)
34. A. Peratt, C, Snell, and L. Thode, IEEE Trans. Plasma Sci., PS-13, 498, (1985)
35. R. Scarpetti and S. Burkhart, IEEE Trans. Plamsa Sci., PS-13, 506, (1985)
36. D. Price et al, IEEE Trans. Plasma Sci., 16, 177, (1988)
37, D. Price et al, Proc. SPIE, Vol 1061, p. 206, (1989)
38. H. Davis et al, Phys. Rev. Let., 55, 2293, (1985)
39. R. Mahaffey et al, Phys. Rev. Let., 39, 843, (1977)
40. T. Kwan et al, Proc. SPIE, vol 873, p62, (1988)
41. H. Davis et al, IEEE Trans. Plasma Sci, 16, 192, (1988)

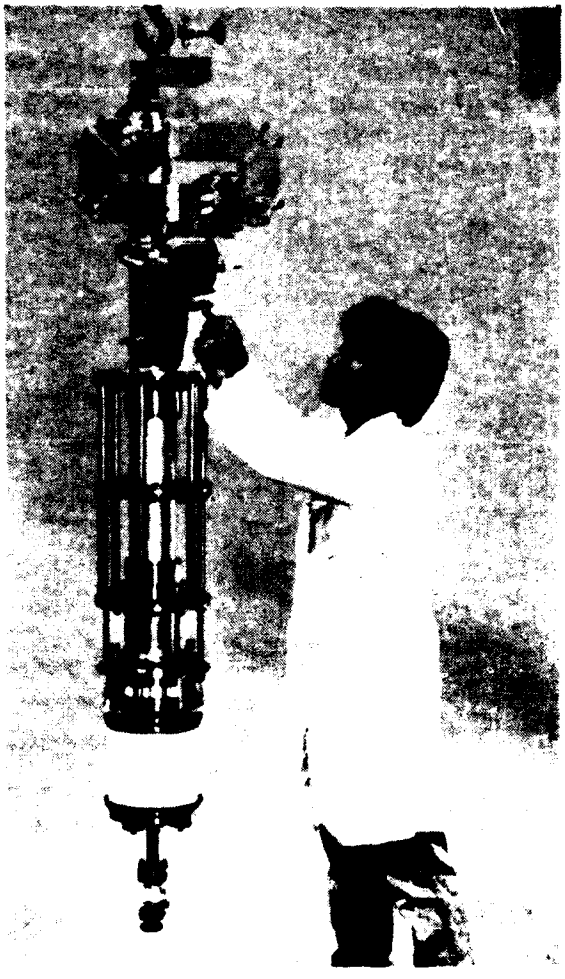

(a)

Fig. 1 — (a) SLAC klystron standing alone, (b) SLAC klystron in the magnet

(b)

Fig. 1 — (Continued) (a) SLAC klystron standing alone, (b) SLAC klystron in the magnet

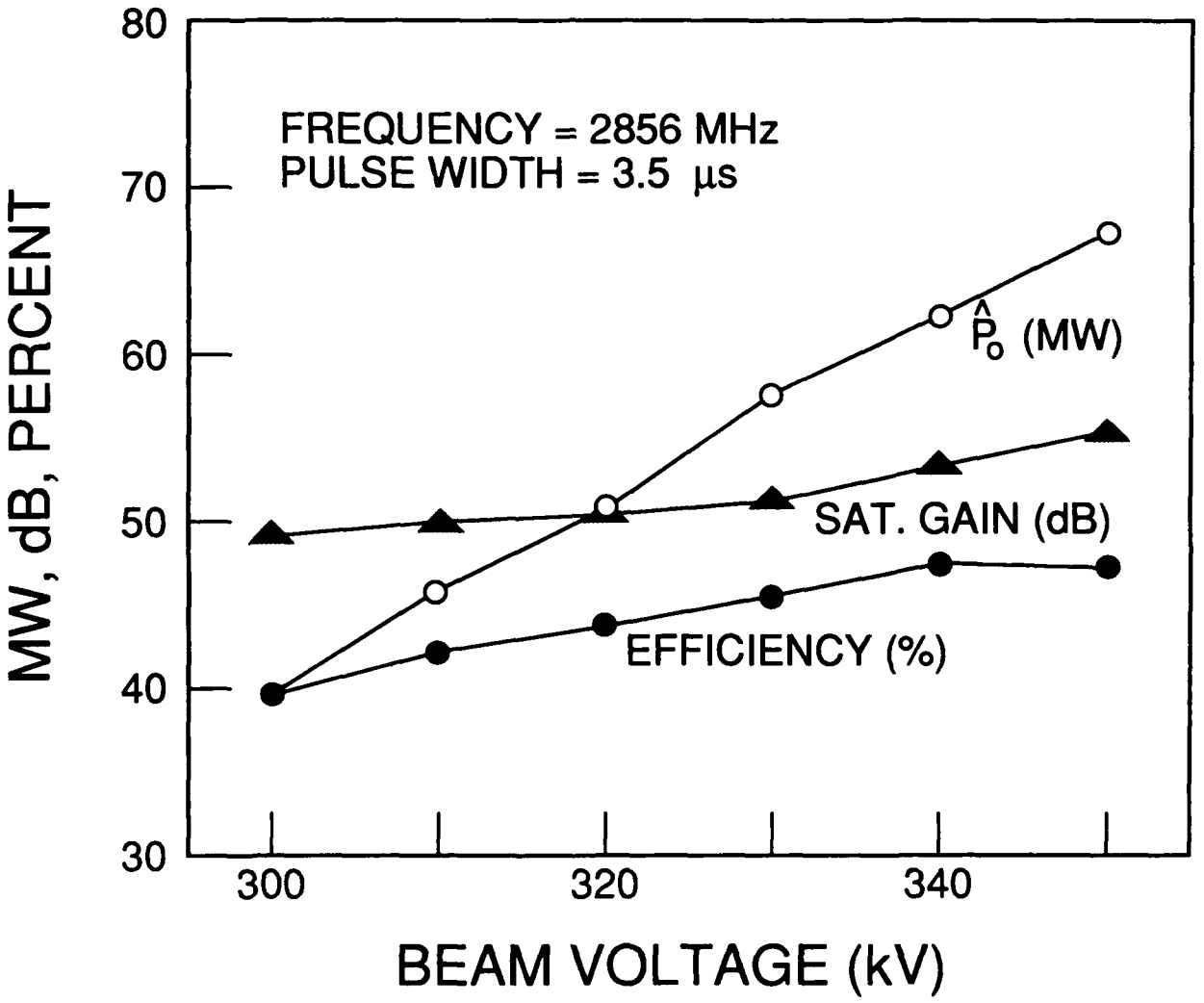

Fig. 2 — Amplification, power and efficiency of a SLAC klystron as a function of voltage

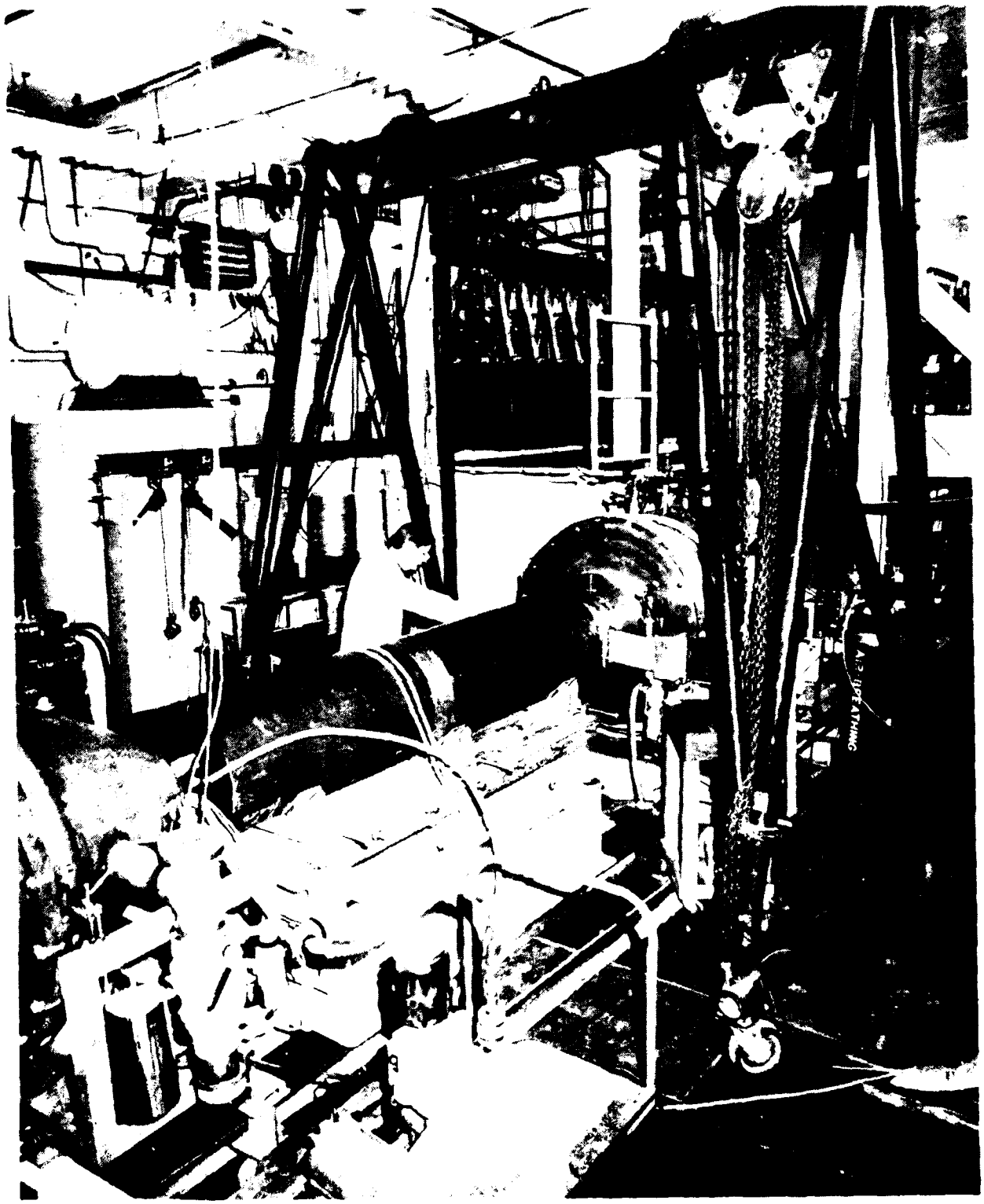

Fig. 3 — The new NRL relativistic klystron facility designed to generate 30 GW of power at 1.3 GHz

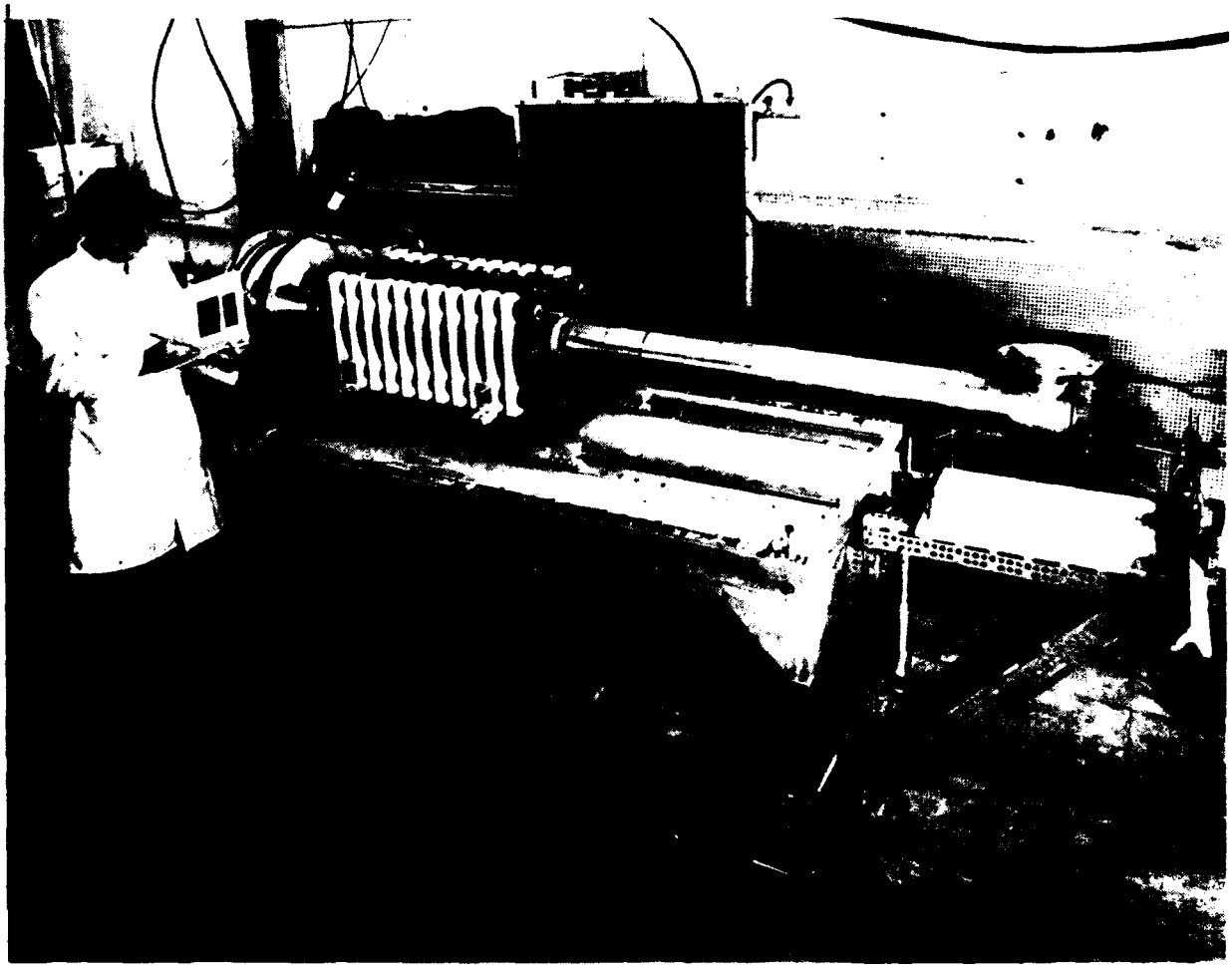

Fig. 4 — The NRL febetron gyrotron

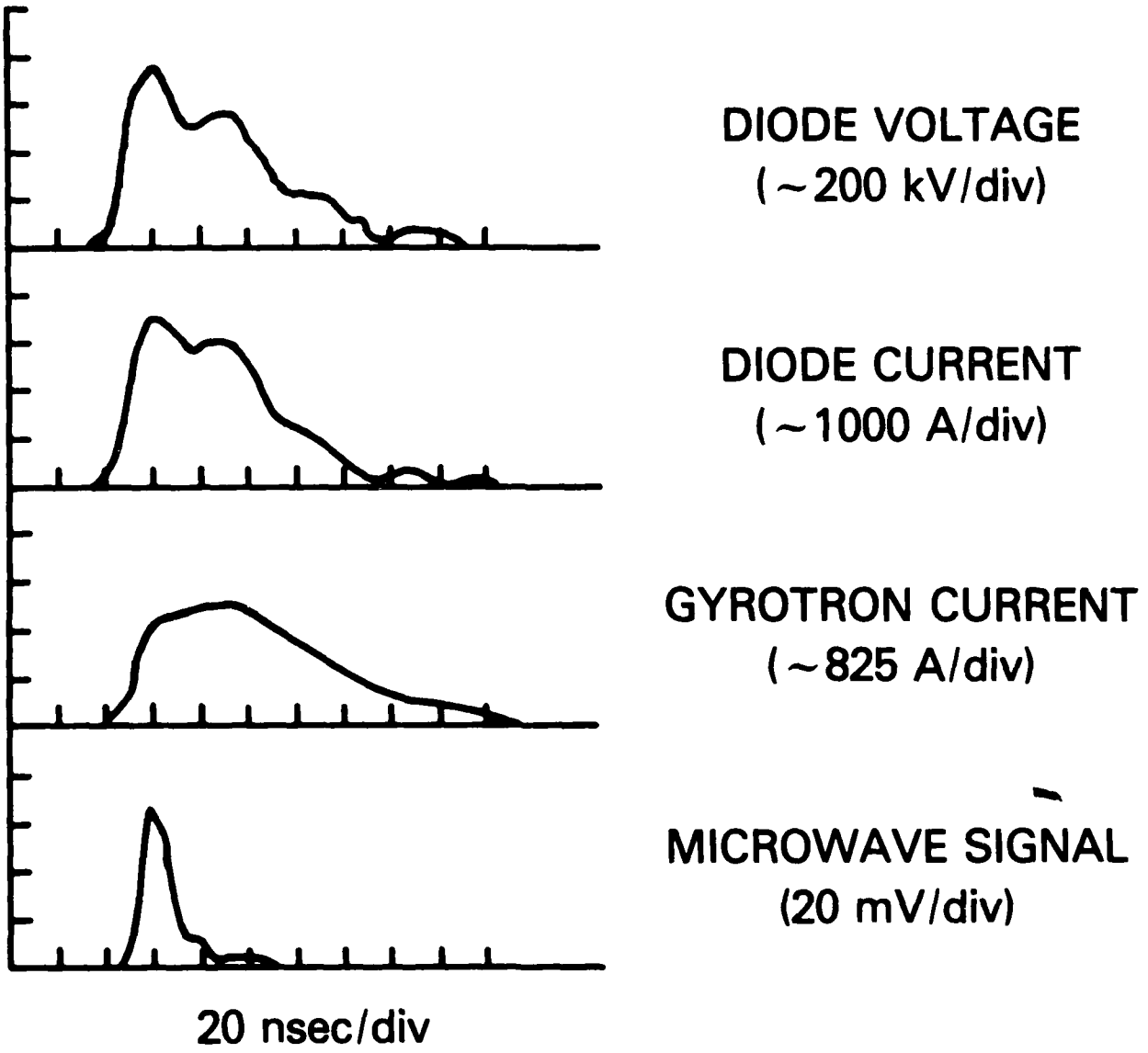

Fig. 5 — The voltage, diode current, gyrotron current and microwave signal as a function of time

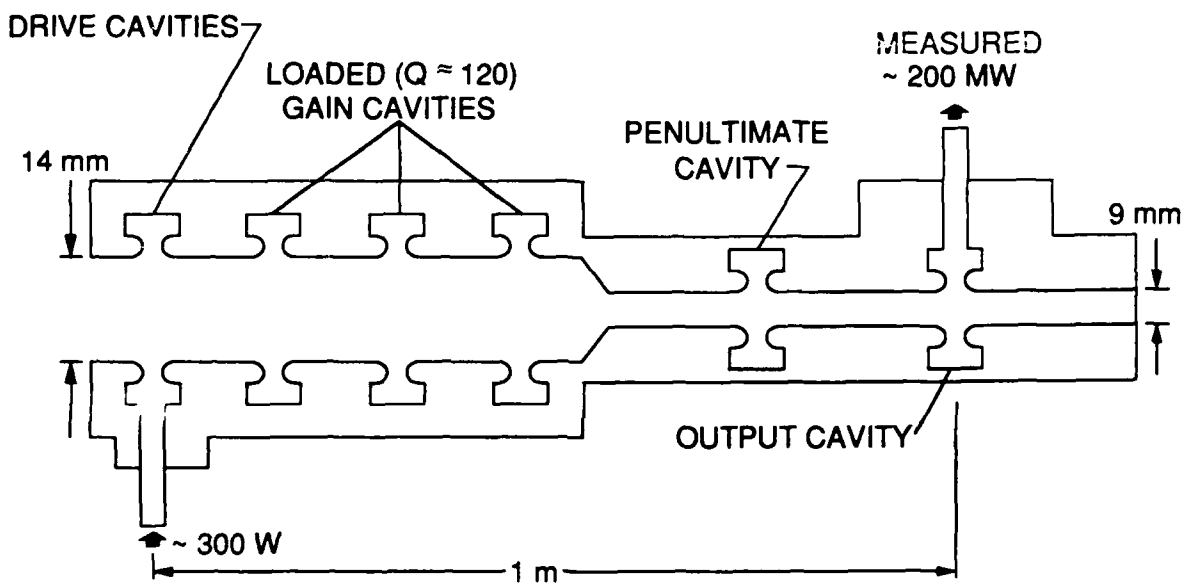

Fig. 6 — Schematic of the relativistic SLAC klystron showing the six cavities used there

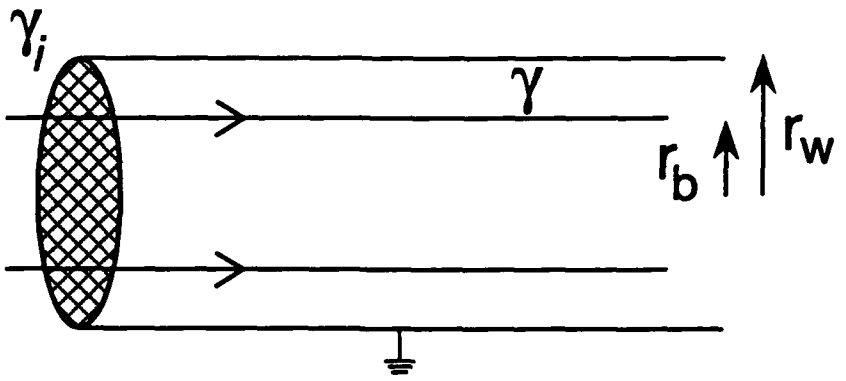

(a)

Fig. 7 — (a) High current electron beam crossing a grounded screen, and (b) the electrostatic potential as a function of distance from the screen

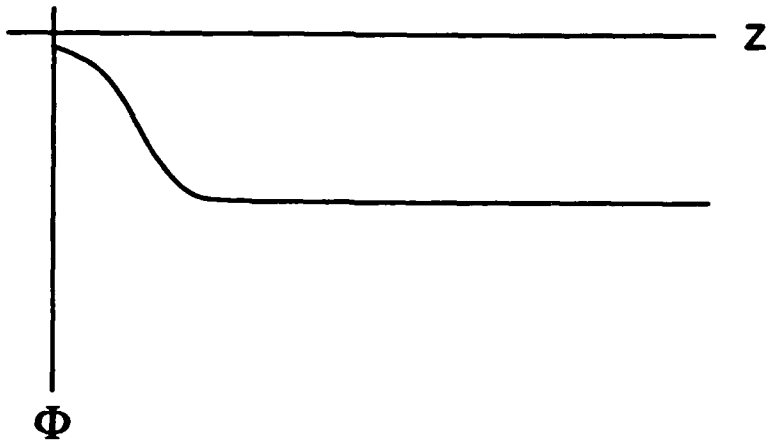

(b)

Fig. 7 — (Continued) (a) High current electron beam crossing a grounded screen, and (b) the electrostatic potential as a function of distance from the screen

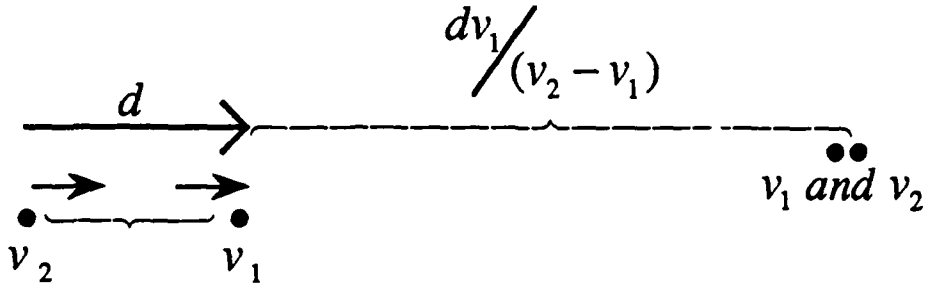

(a)

Fig. 8 — (a) Two electron orbits in free space and bunching further down the drift region, (b) the same two electrons bunching in a shorter distance after crossing a potential barrier

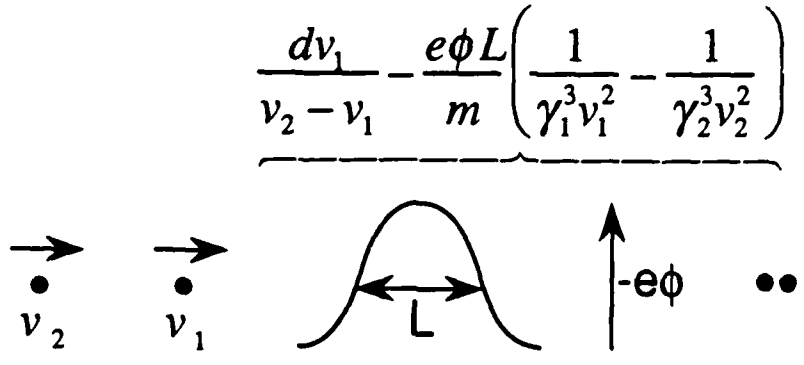

(b)

Fig. 8 — (Continued) (a) Two electron orbits in free space and bunching further down the drift region, (b) the same two electrons bunching in a shorter distance after crossing a potential barrier

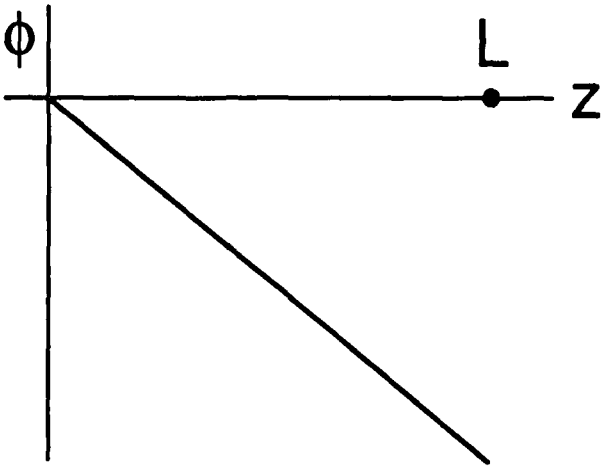

(a)

Fig. 9 — The effective rf electrostatic potential across an accelerating gap in (a) the absence, and (b) the presence of strong self fields

b)

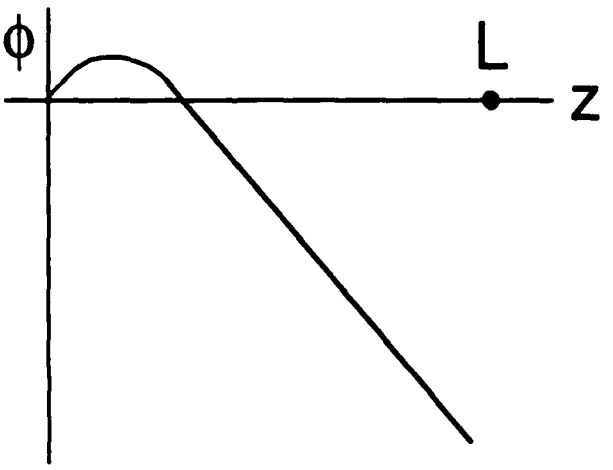

(b)

Fig. 9 — (Continued) The effective rf electrostatic potential across an accelerating gap in (a) the absence, and (b) the presence of strong self fields

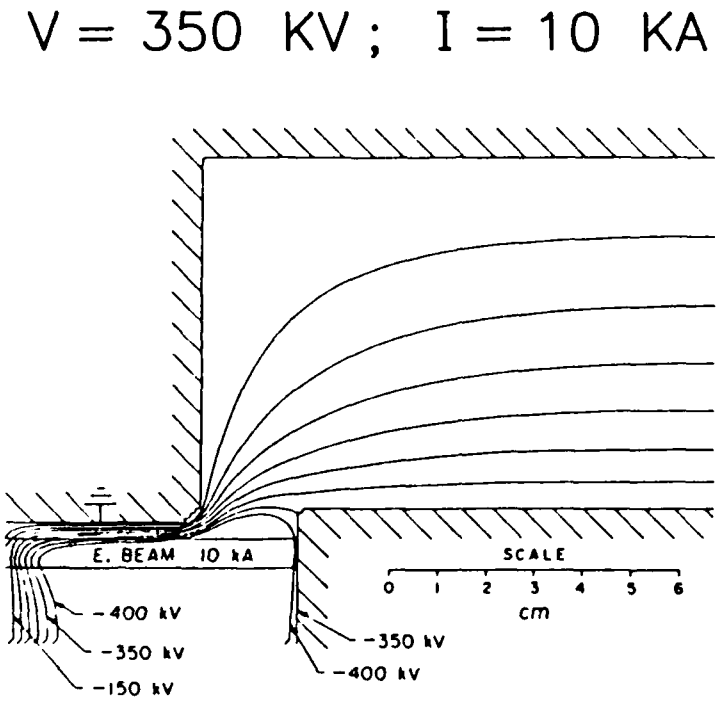

(a)

Fig. 10 — Computer plot of the potential in the NRL relativistic klystron at currents of (a) 10 kA and (b) no current

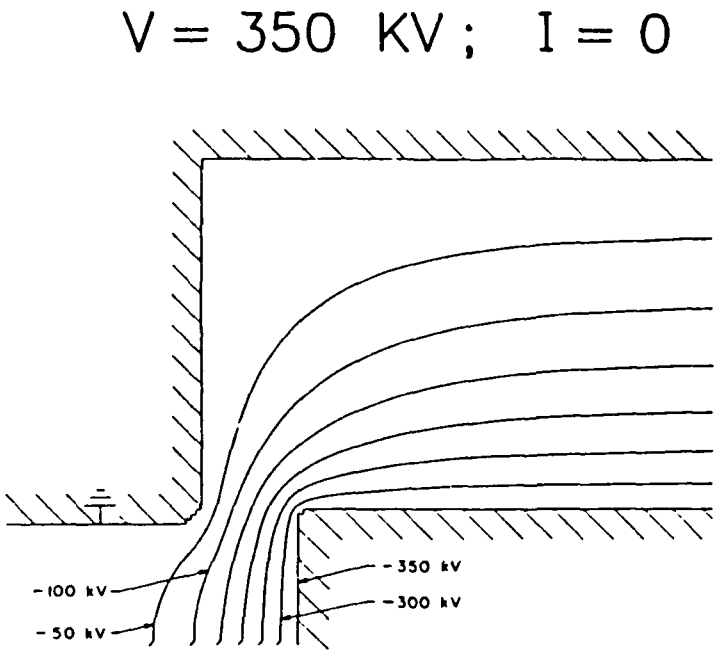

(b)

Fig. 10 — (Continued) Computer plot of the potential in the NRL relativistic klystron at currents of (a) 10 kA and (b) no current

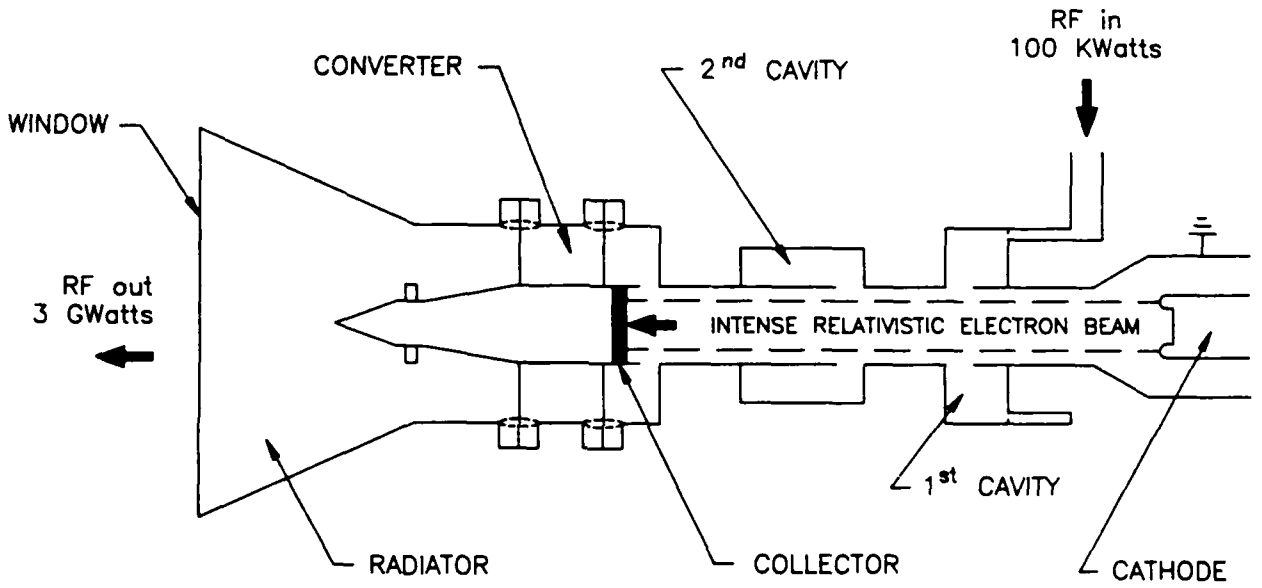

Fig. 11 — Schematic of the NRL relativistic klystron

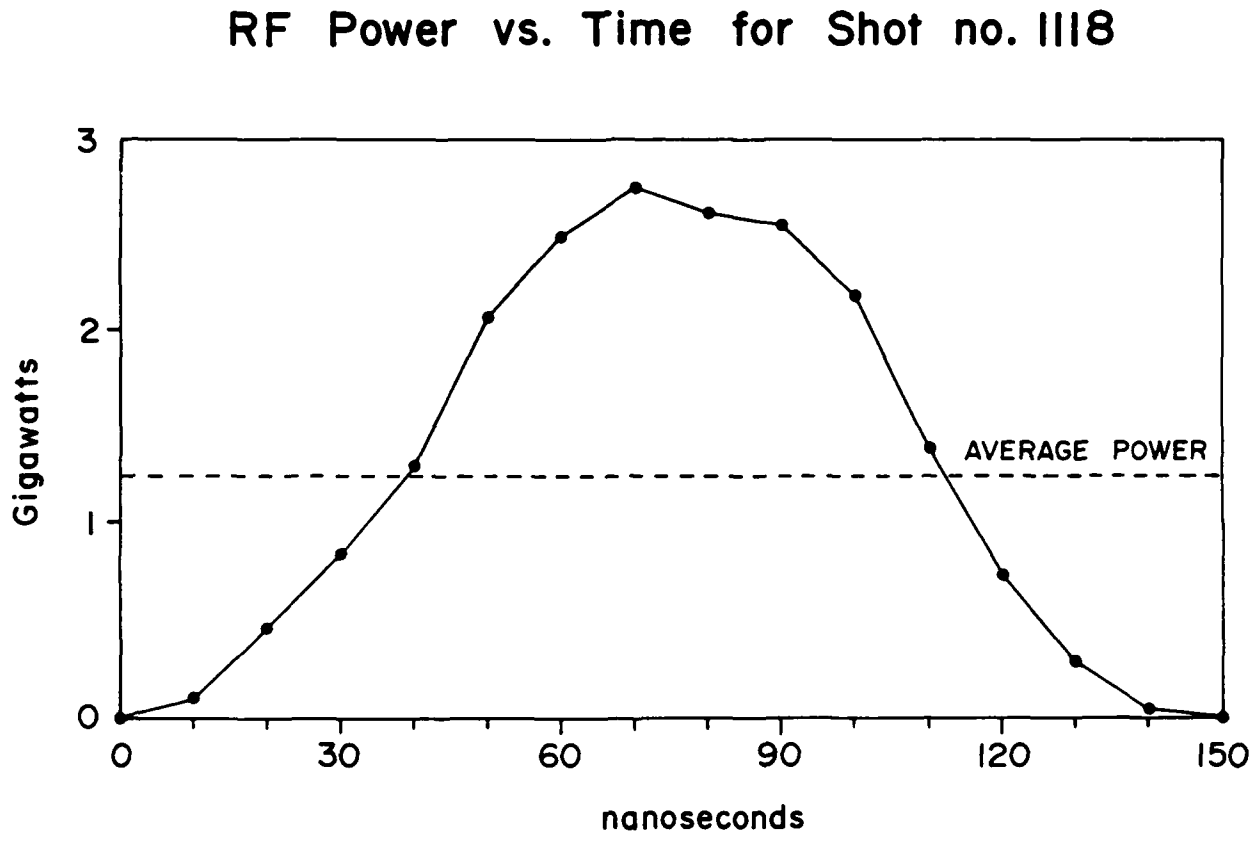

Fig. 12 — Power of the NRL relativistic klystron during an RF pulse

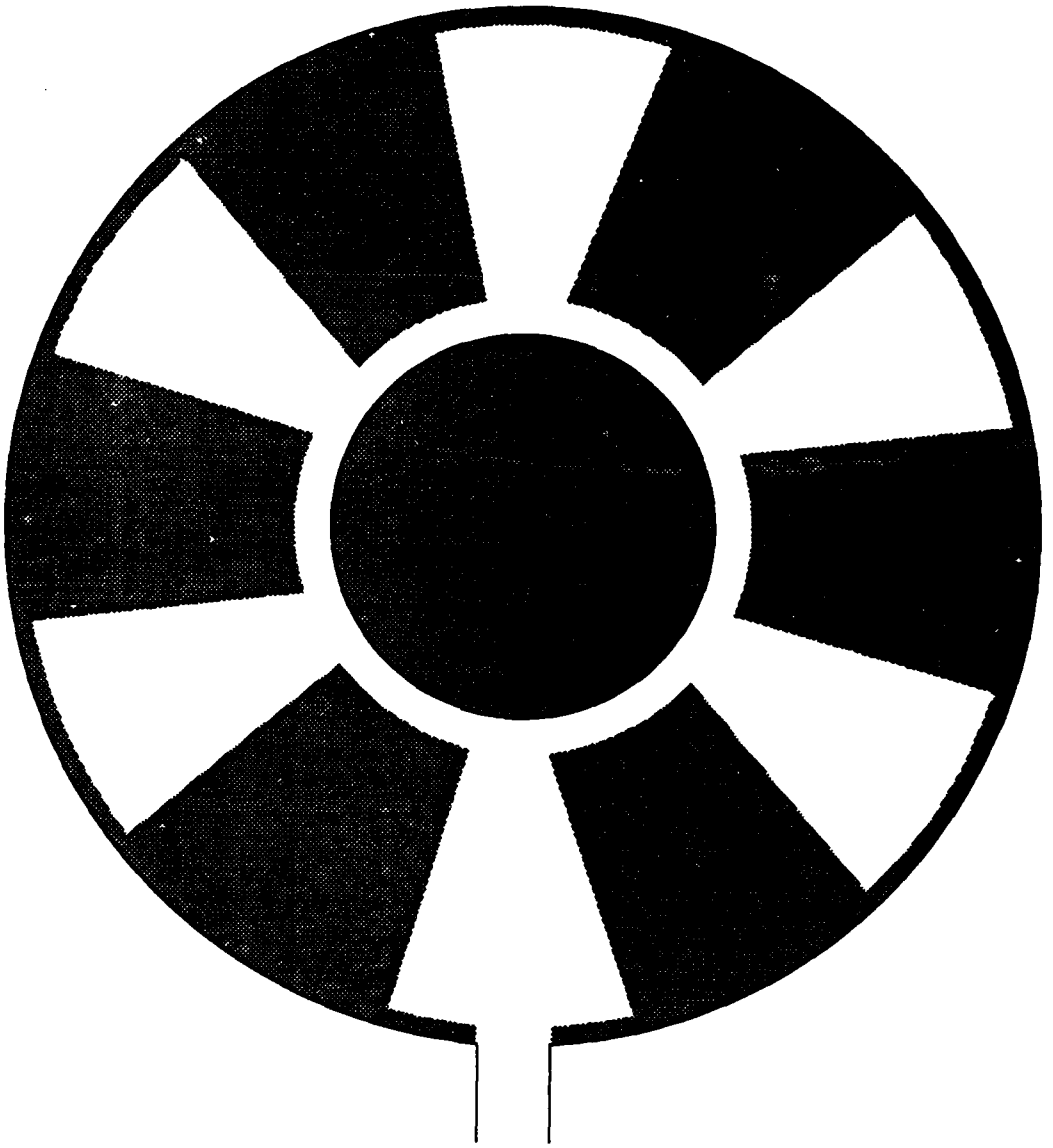

(a)

Fig. 13 — (a) Cylindrical, and (b) planar configuration of the magnetron

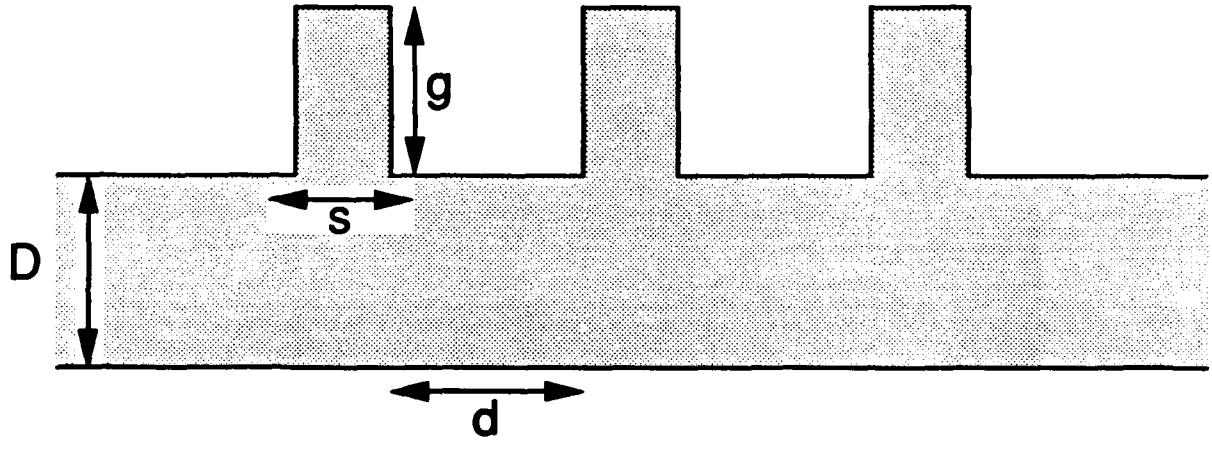

(b)

Fig. 13 — (Continued) (a) Cylindrical, and (b) planar configuration of the magnetron

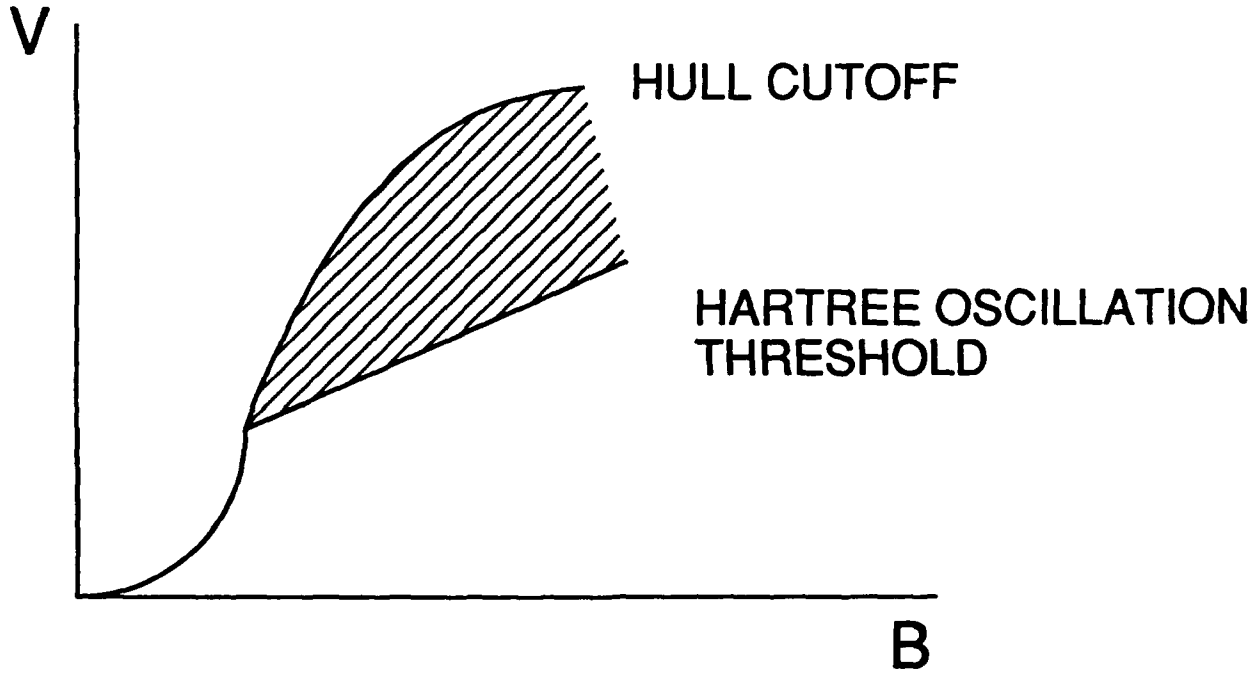

Fig. 14 — Operating regime of the magnetron-on in (V,B) space. The upper curve is the Hull cutoff, the lower one is the Hartree-Buneman oscillation threshold

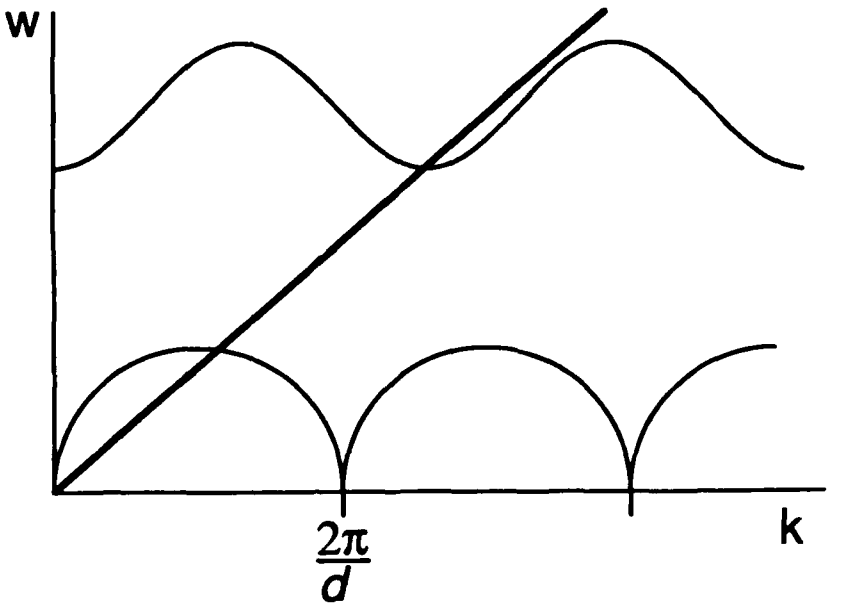

(a)

Fig. 15 — Comparison of smooth wall and rippled wall dispersion relations for the (a) transmission line, and (b) waveguide modes

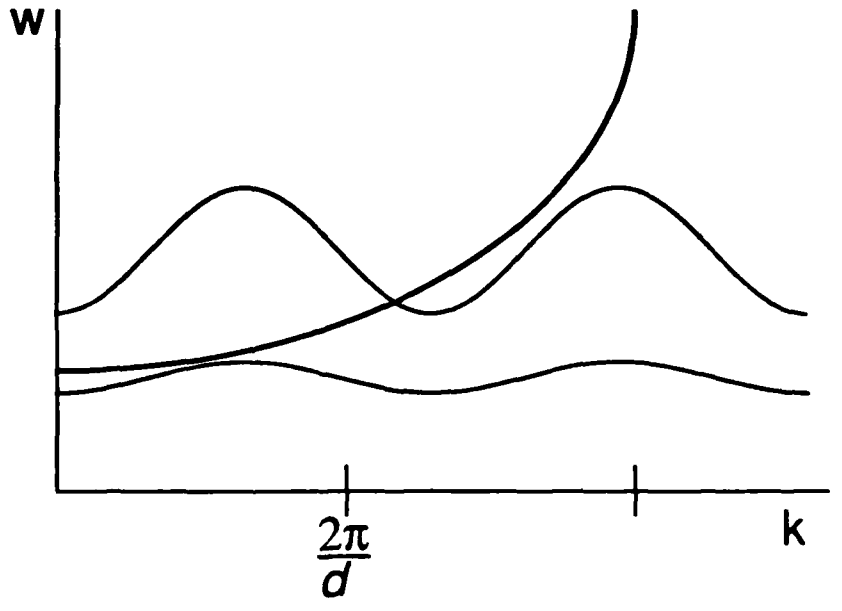

(b)

Fig. 15 — (Continued) Comparison of smooth wall and rippled wall dispersion relations for the (a) transmission line, and (b) waveguide modes

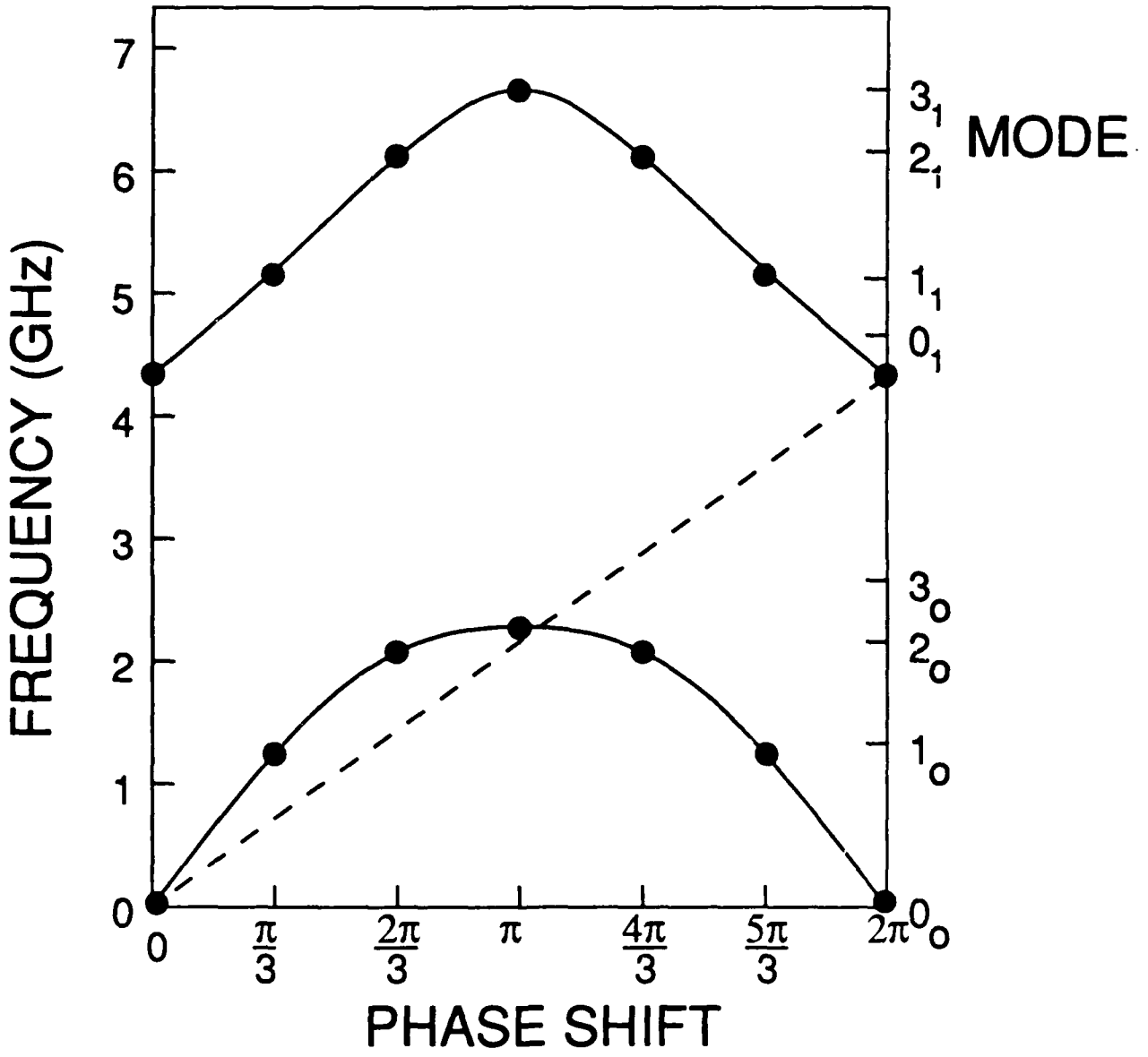

Fig. 16 — Dispersion relation of the A-6 magnetron

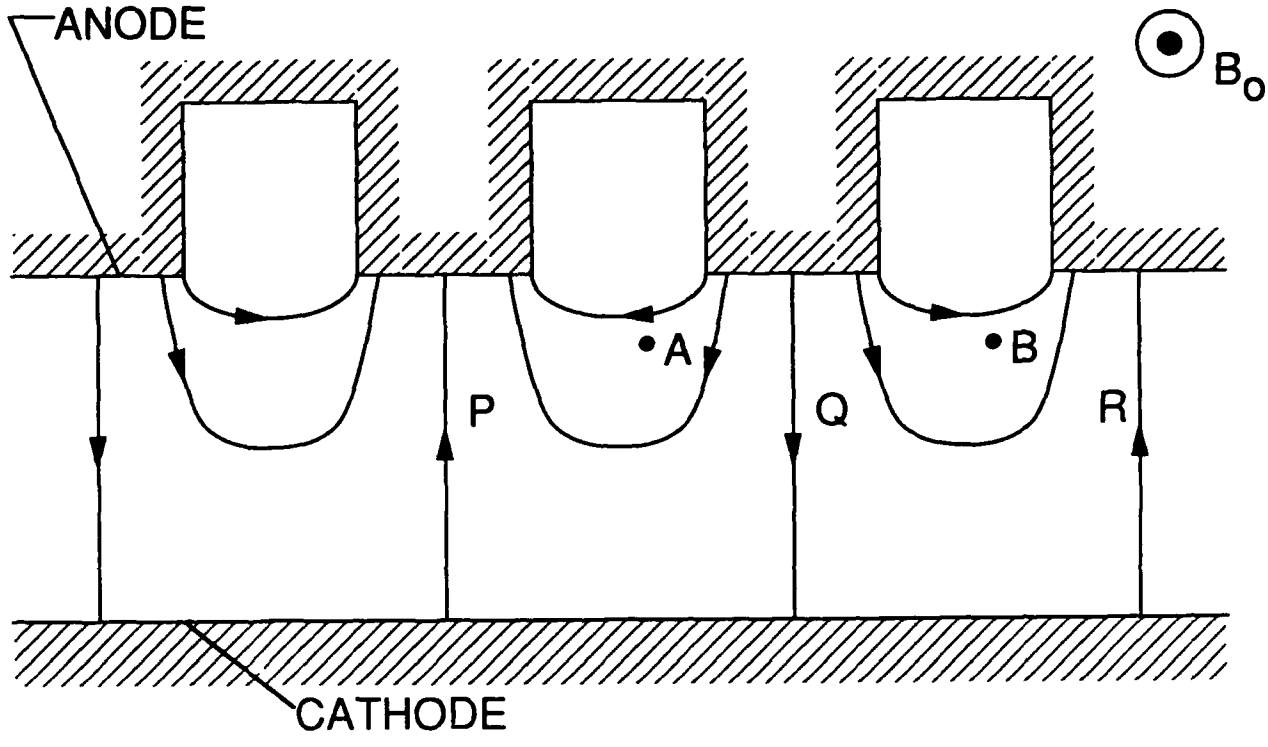

Fig. 17 — Planar version of the magnetron showing the field lines at a particular time in the π mode

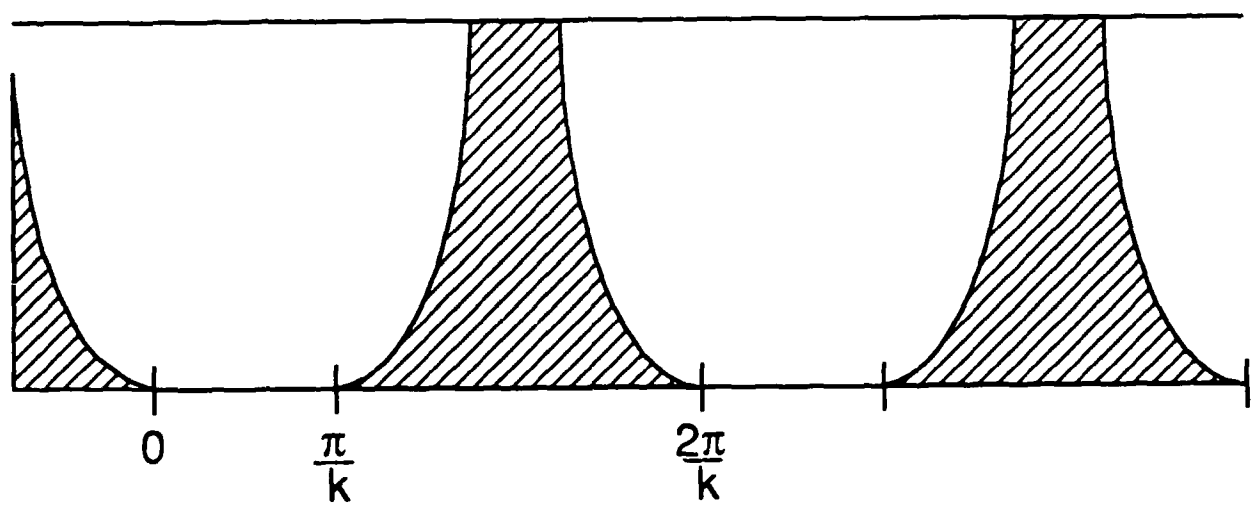

Fig. 18 — Plot of boundaries of the electron spokes (shaded region) in a smooth bore magnetron

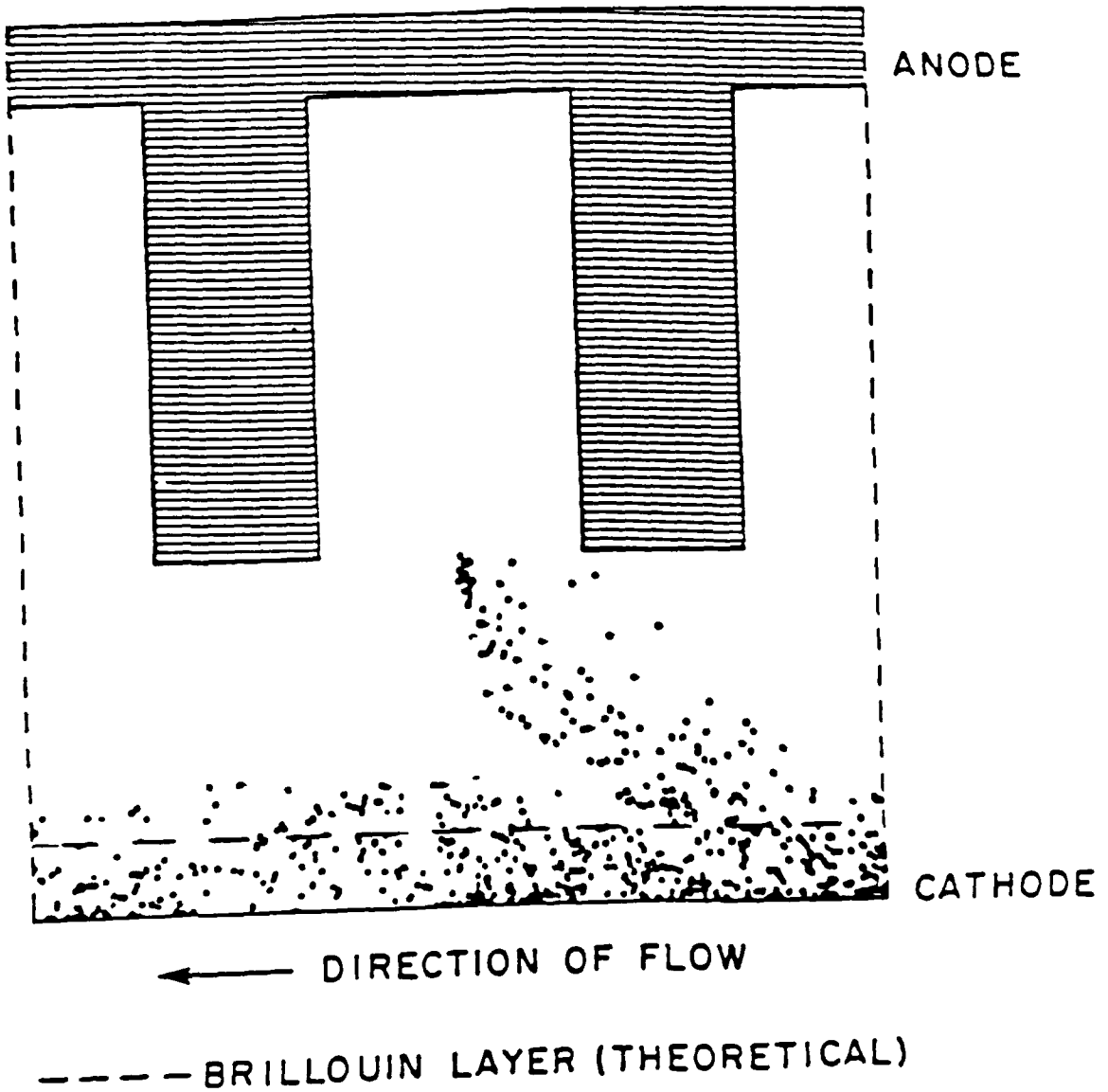

Fig. 19 — Particle simulation of spoke formation in the magnetron

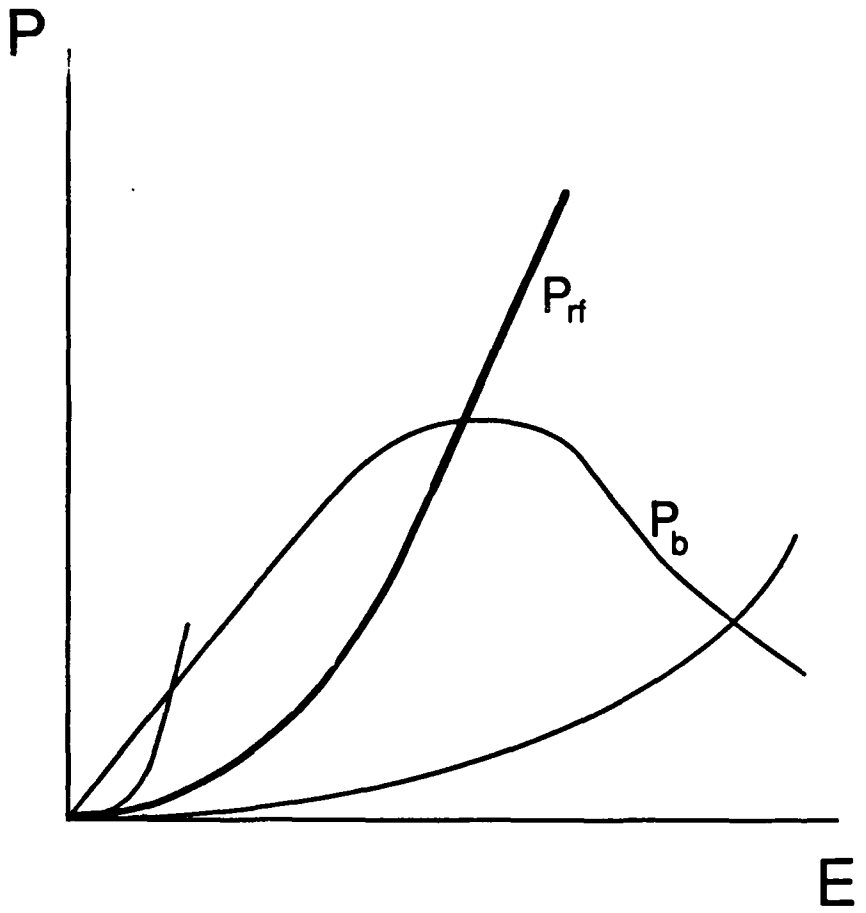

Fig. 20 — Plot of beam power loss and RF power output as a function of RF field amplitude ϕ_0. The output is shown for three different values of cavity Q.

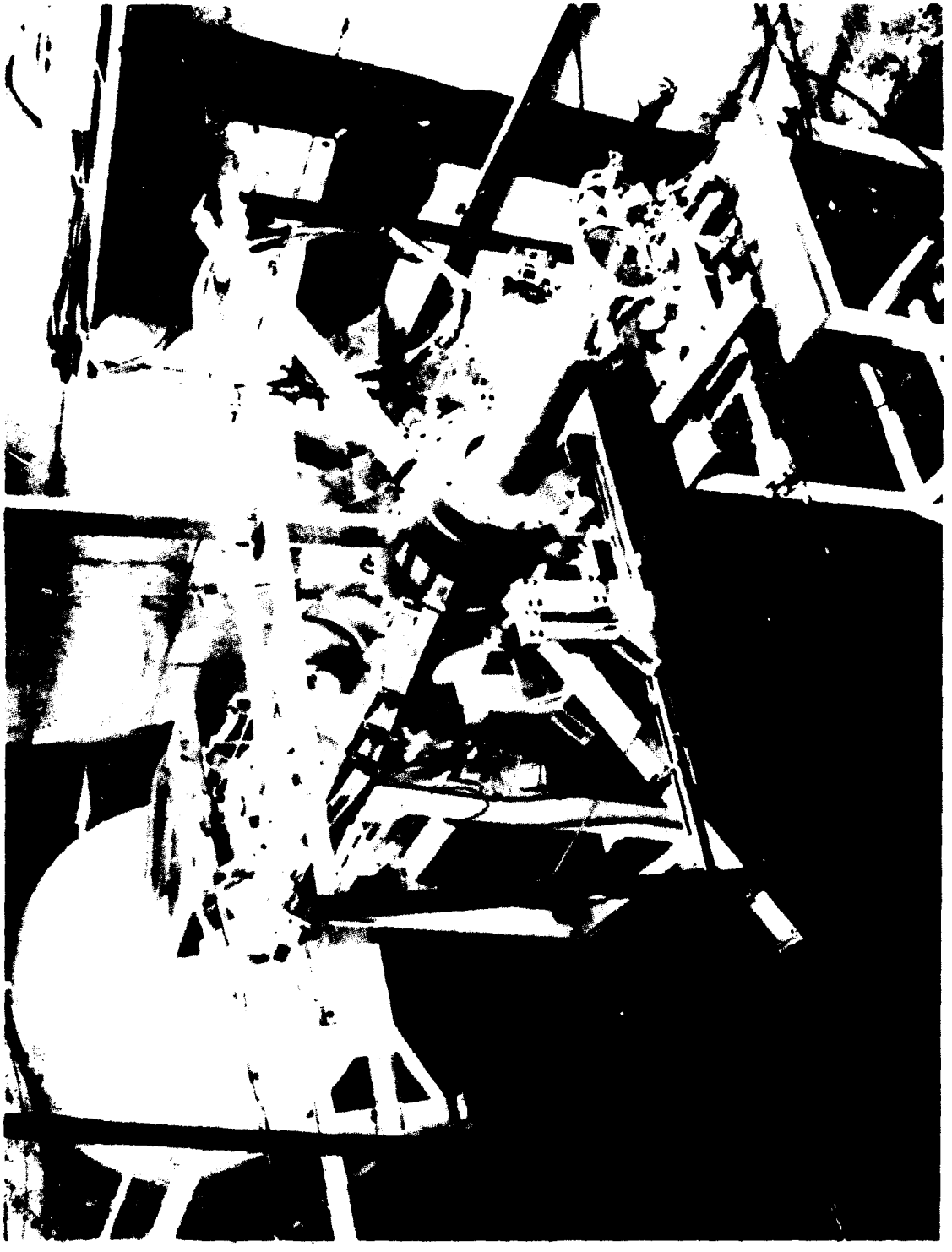

Fig. 21 — A photograph of the magnetron set up a Physics International Company

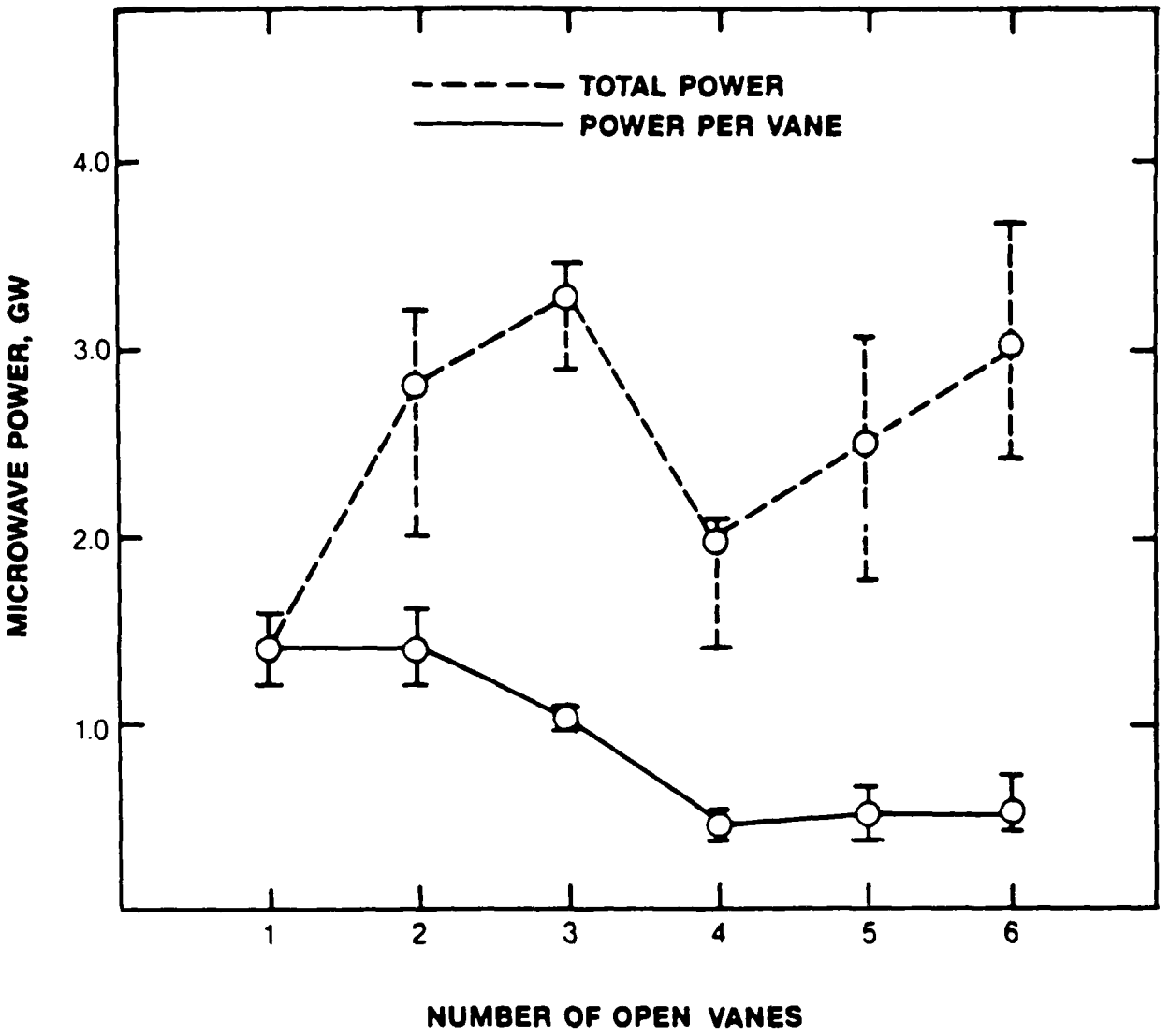

Fig. 22 — Power of the PI magnetron as a function of the number of vanes for which output is extracted

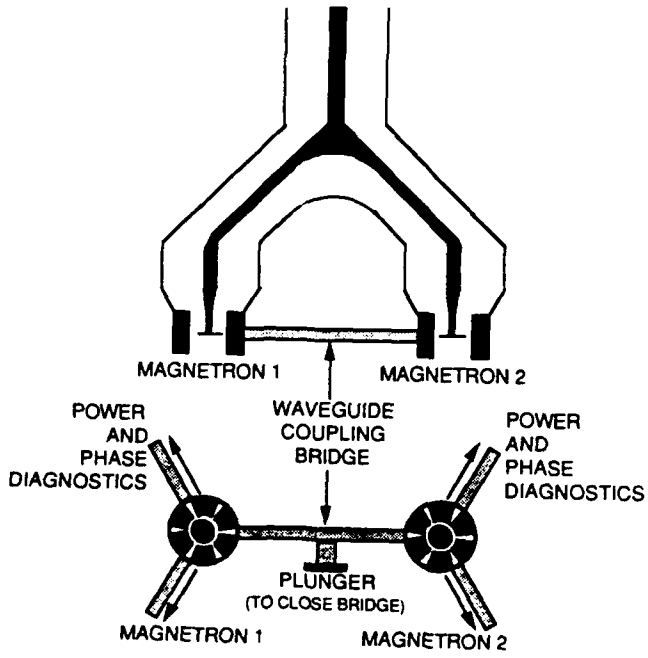

(a)

Fig. 23 — (a) Schematic of the PI phase locked experiment, (b) the relative phase as a function of time

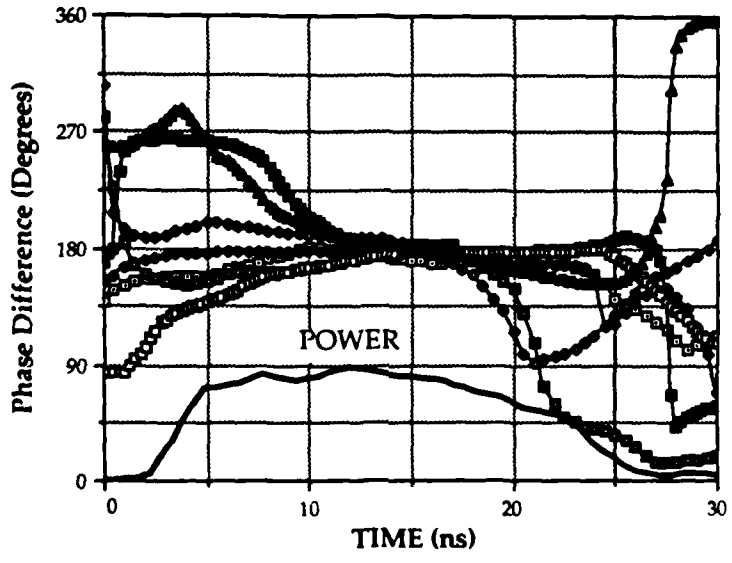

(b)

Fig. 23 — (Continued) (a) Schematic of the PI phase locked experiment, (b) the relative phase as a function of time

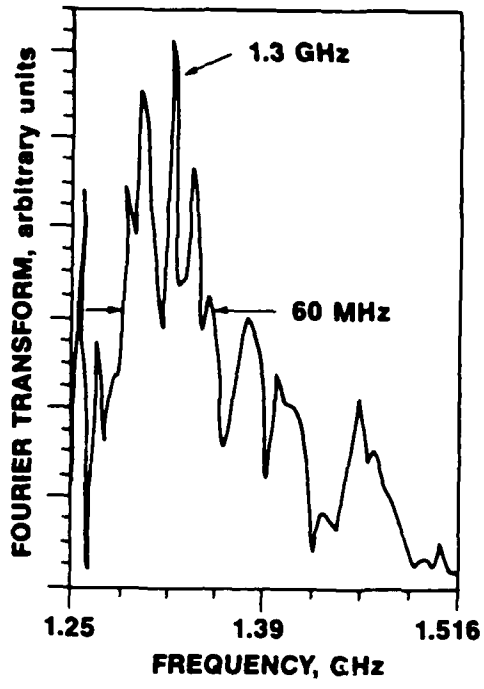

(a)

Fig. 24 — Spectrum of a vircator (a) without, and (b) with a cavity

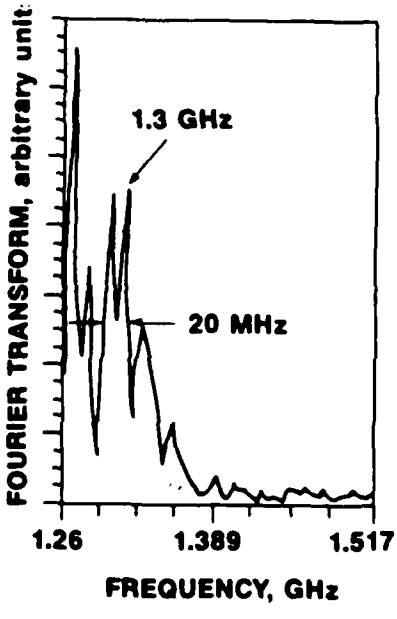

(b)

Fig. 24 — (Continued) Spectrum of a vircator (a) without, and (b) with a cavity

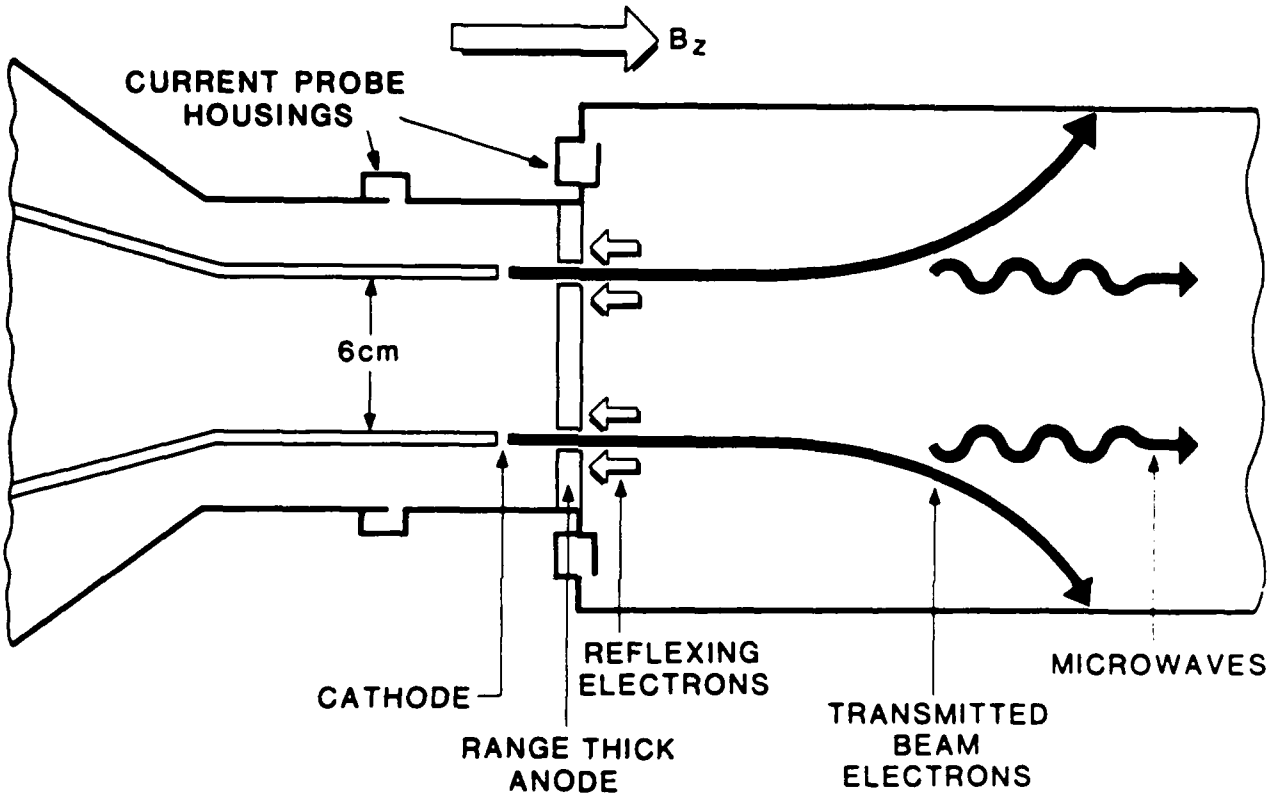

Fig. 25 — Schematic of the Los Alamos Reditron

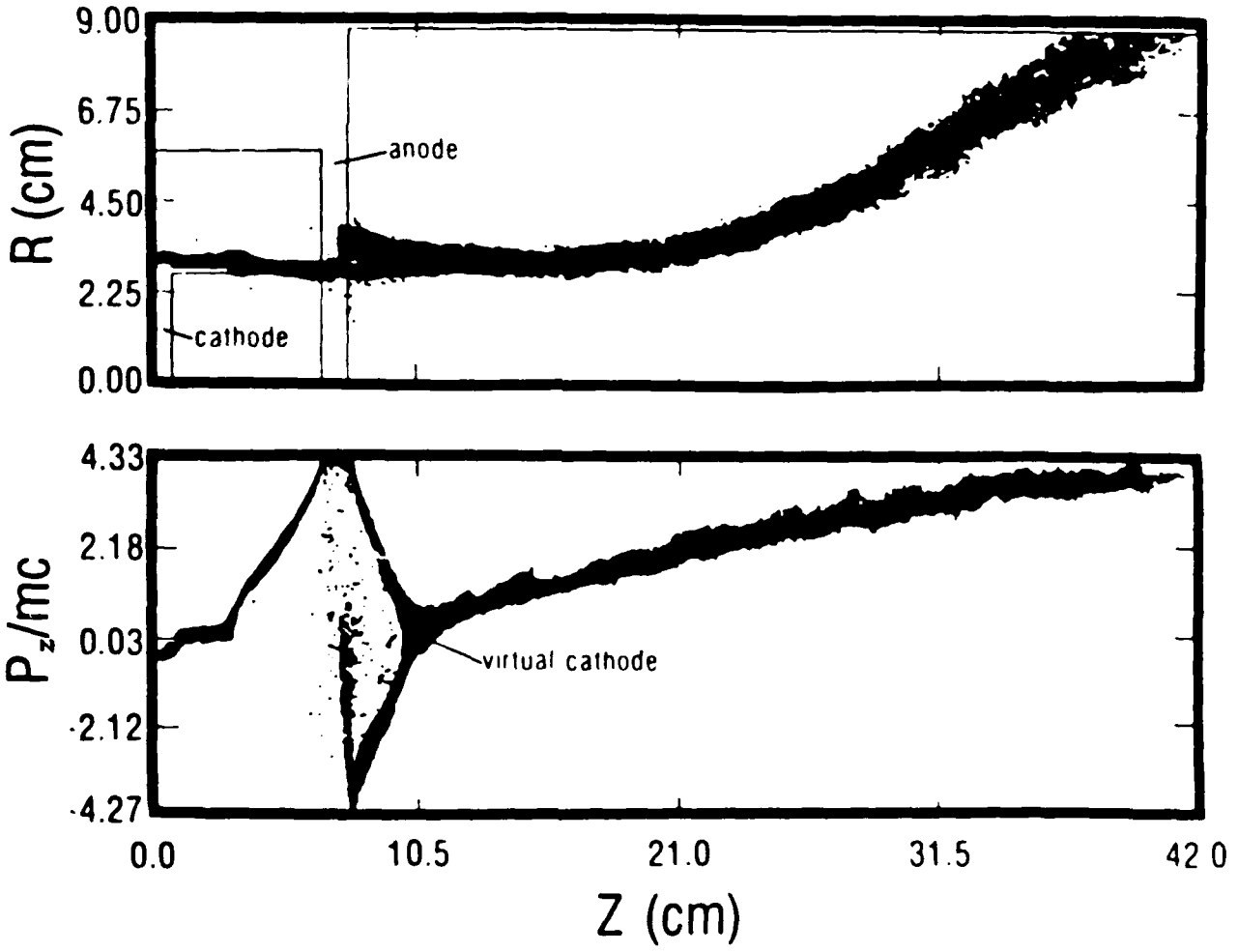

Fig. 26 — Particle simulation of the reditron

DISTRIBUTION LIST

Air Force Avionics Laboratory
AFWAL/AADM-1
Wright/Patterson AFB, Ohio 45433
Attn: Walter Friez — 1 copy

Air Force Office of
Scientific Research
Bolling AFB
Washington, D.C. 20332
Attn: H. Schlossberg
R. Barker — 1 copy

Air Force Weapons Lab
Kirkland AFB
Albuquerque, New Mexico 87117
Attn: Dr. William Baker
Dr. Brendan Godfrey — 2 copies

ALCOA Defense Systems Inc.
16761 Via Del Campo Court
San Diego, CA 92127
Attn: H. Buscher — 1 copy

Battelle Memorial Institute
505 King Ave
Columbus, Ohio 43201
Attn: V. Puglielli, Room 4133 — 2 copies

Columbia University
520 West 120th Street
Department of Electrical Engineering
New York, N.Y. 10027
Attn: Dr. S.P. Schlesinger
A. Sen — 1 copy

Columbia University
520 West 120th Street
Department of Applied Physics
and Nuclear Engineering
New York, New York 10027
Attn: T.C. Marshall
R. Gross — 1 copy

Cornell University
School of Applied and Engineering Physics
Ithica, New York 14853
Attn: Prof. Hans H. Fleischmann — 1 copy

John Nation — 1 copy
R. N. Sudan — 1 copy
David Hammer

Dartmouth College
18 Wilder, Box 6127
Hanover, New Hampshire 03755
Attn: Dr. John E. Walsh — 1 copy

Department of Energy
Washington, D.C. 20545
Attn: T.V. George/ER-531, GTN — 1 copy

Defense Advanced Research Project Agency/DEO
1400 Wilson Blvd.
Arlington, Virginia 22209
Attn: Dr. B. Hui — 1 copy
Dr. L. Buchanan — 1 copy

Defense Communications Agency
Washington, D.C. 20305
Attn: Dr. Pravin C. Jain
Assistant for Communications
Technology — 1 copy

Defense Nuclear Agency
Washington, D.C. 20305
Attn: Mrs Joan Pierre — 1 copy

Defense Technical Information Center
Cameron Station
5010 Duke Street
Alexandria, Virginia 22314 — 2 copies

Georgia Tech. EES-EOD
Baker Building
Atlanta, Georgia 30332
Attn: Dr. James J. Gallagher — 3 copies
Dr. Robert McMillan

Hanscomb Air Force Base
Stop 21, Massachusetts 01731
Attn: Lt. Rich Nielson/ESD/INK — 1 copy
Dr. Dallas Hayes

Hughes Aircraft Co.
Electron Dynamics Division
3100 West Lomita Boulevard

Torrance, California 90509
Attn: J. Christiansen — 1 copy
J.J. Tancredi — 1 copy

Hughes Aircraft Company
Electro-Optical and Data systems Group
Bldg E. 55, MS G206
1250 Rosecrans
El Segundo, CA 90245
Attn: J.J. Thomson

KMS Fusion, Inc.
3941 Research Park Dr.
P.O. Box 1567
Ann Arbor, Michigan 48106
Attn: S.B. Segall — 1 copy

Lawrence Livermore National Laboratory
P.O. Box 808
Livermore, California 94550
Attn: Dr. D. Prosnitz — 1 copy
Dr. T.J. Orzechowski — 1 copy
Dr. J. Chase — 1 copy
Dr. M. Caplan — 1 copy

Litton Electron Devices
960 Industrial Road
San Carlos, CA 94070-4194
Attn: Dr. Robert Symons — 1 copy

Los Alamos Scientific Laboratory
P.O. Box 1663, AT5-827
Los Alamos, New Mexico 87545
Attn: Dr. J.C. Goldstein — 1 copy
Dr. T.J.T. Kwan — 1 copy
Dr. L. Thode — 1 copy
Dr. R. R. Bartsch — 1 copy
Dr. H. Davies — 1 copy

Massachusetts Institute of Technology
Department of Physics
Cambridge, Massachusetts 02139
Attn: Dr. G. Bekefi/36-213 — 1 copy
Dr. M. Porkolab/NW 36-213 — 1 copy
Dr. R. Davidson/NW 16-206 — 1 copy

Massachusetts Institute of Technology
167 Albany St., N.W. 16-200

Cambridge, Massachusetts 02139	
Attn: Dr. R. Temkin/NW 14-4107	1 copy
Dr. B. Danley	1 copy
Dr. K Kreischer	1 copy
Spectra Technologies	
2755 Northup Way	
Bellevue, Washington 98004	
Attn: Dr. J.M. Slater	1 copy
Mission Research Corporation	
Suite 201	
5503 Cherokee Avenue	
Alexandria, Virginia 22312	
Attn: Dr. M. Bollen	1 copy
Mission Research Corporation	
1720 Randolph Road, S.E.	
Albuquerque, New Mexico 87106	
Attn: Dr. Donald Sullivan	1 copy
SPAWAR	
Washington, D.C. 20363-5100	
Attn: E. Warden	
Code PDE 106-3113	1 copy
CDR Michael Kaiser	
PMW 145	1 copy
Naval Research Laboratory	
Addressee: Attn: Name/Code	
Code 1001 - T. Coffey	1 copy
Code 1220 - Security	1 copy
Code 2628 - TID Distribution	22 copies
Code 4000 - W. Ellis	1 copy
Code 4600 - D. Nagel	1 copy
Code 4650 - T. Wieting	1 copy
Code 4700 - S. Ossakow	26 copies
Code 4795 - C. Kapetanakos	1 copy
Code 4707 - W. Manhiemer	100 copies
Code 4793 - W. Black	1 copy
Code 4794 - A. Fliflet	1 copy
Code 4793 - S. Gold	1 copy
Code 4793 - A. Kinkead	1 copyy
Code 4794 - M. Rhinewine	1 copy
Code 4770 - G. Cooperstein	1 copy
Code 4780 - A.W. Ali	1 copy
Code 4790 - Branch Office	10 copies
Code 4790 - C.M. Hui	1 copy
Code 4790 - Y.Y. Lau	1 copy

Code 4790 - P. Sprangle	1 copy
Code 5300 - M. Skolnik	1 copy
Code 5700 - J. Montgomery	1 copy
Code 6840 - S.Y. Ahn	1 copy
Code 6840 - A. Ganguly	1 copy
Code 6840 - R.K. Parker	1 copy
Code 6840 - N.R. Vanderplaats	1 copy
Code 6850 - L.R. Whicker	1 copy
Code 6875 - R. Wagner	1 copy

Naval Surface Warfare Center
Route 206
Dahlgren, VA 22448
Attn: M.T. Houghton
F-12 Bld 424T — 2 copies

Naval Weapons Center
China Lake, CA 93555
Attn: David Wagner
Code 3521 — 2 copies

Northrop Corporation
Defense Systems Division
600 Hicks Rd.
Rolling Meadows, Illinois 60008
Attn: Dr. Gunter Dohler — 1 copy

Oak Ridge National Laboratory
P.O. Box Y
Mail Stop 3
Building 9201-2
Oak Ridge, Tennessee 37830
Attn: Dr. A. England — 1 copy

Office of Naval Research
800 N. Quincy Street
Arlington, Va. 22217
Attn: Dr. C. Roberson — 1 copy

Office of Naval Technology
800 North Quincy Street
Arlington VA 22217-5000
Attn: Dr. E. Zimet — 1 copy
Dr. J. Hall — 1 copy

Optical Sciences Center
University of Arizona
Tucson, Arizona 85721
Attn: Dr. Willis E. Lamb, Jr. — 1 copy

OSD/SDIO
Attn: IST (Dr. H. Brandt)
Washington, D.C. 20301-7100 — 5 copies

Pacific Missile Test Center
Code 0141-5
Point Muga, California 93042
Attn: Will E. Chandler — 1 copy

Physical Dynamics, Inc.
P.O. Box 10367
Oakland, California 94610
Attn: A. Thomson — 1 copy

Physics International
2700 Merced Street
San Leandro, California 94577
Attn: Dr. J. Benford — 3 copies

Princeton Plasma
Plasma Physics Laboratory
James Forrestal Campus
P.O. Box 451
Princeton, New Jersey 08544
Attn: Dr. R. Perkins — 1 copy
Dr. H. Hsuan — 1 copy

Raytheon Company
Microwave Power Tube Division
Foundry Avenue
Waltham, Massachusetts 02154
Attn: N. Dionne — 1 copy
A. Palevsky — 1 copy

Sandia National Laboratories
ORG. 1231, P.O. Box 5800
Albuquerque, New Mexico 87185
Attn: Dr. Thomas P. Wright — 1 copy
Mr. J.E. Powell — 1 copy
Dr. J. Hoffman — 1 copy
Dr. W.P. Ballard — 1 copy
Dr. C. Clark — 1 copy

Science Applications, Inc.
1710 Goodridge Dr.
McLean, Virginia 22102
Attn: Adam Drobot — 1 copy

D. Bacon — 1 copy

Stanford University
High Energy Physics Laboratory
Stanford, California 94305
Attn: Dr. T.I. Smith — 1 copy
Dr. Matt Allen — 1 copy

TRW, Inc.
Space and Technology Group
Suite 2600
1000 Wilson Boulevard
Arlington, VA 22209
Attn: Dr. Neil C. Schoen — 1 copy

TRW, Inc.
Redondo Beach, California 90278
Attn: Dr. H. Boehmer — 1 copy
Dr. T. Romisser — 1 copy

University of California
Physics Department
Irvine, California 92717
Attn: Dr. G. Benford — 1 copy
Dr. N. Rostoker — 1 copy

University of California
Department of Physics
Los Angeles, CA 90024
Attn: Dr. A.T. Lin — 1 copy
Dr. N. Luhmann — 1 copy
Dr. D. McDermott — 1 copy

University of Cincinnati
Cincinatti, Ohio, 45221
Deprtment of Electrical and Computer Engineering
Attn: Prof A. Ferendeci — 1 copy

University of Maryland
Department of Electrical Engineering
College Park, Maryland 20742
Attn: Dr. V. L. Granatstein — 1 copy
Dr. W. W. Destler — 1 copy

University of Maryland
Laboratory for Plasma Research
College Park, Maryland 20742
Attn: Dr. John Finn — 1 copy
Dr. Baruch Levush — 1 copy

Dr. Tom Antonsen — 1 copy
Dr. Edward Ott — 1 copy

University of Michigan
Department of Nuclear Engineering
Ann Arbor, Michigan, 48109
Attn: Prof R. Gilgenbach — 1 copy

University of Tennessee
Dept. of Electrical Engr.
Knoxville, Tennessee 37916
Attn: Dr. I. Alexeff — 1 copy

University of New Mexico
Department of Physics and Astronomy
800 Yale Blvd, N.E.
Albuquerque, New Mexico 87131
Attn: Dr. Gerald T. Moore — 1 copy
Dr. Stan Humphries — 1 copy

University of Utah
Deparment of Electrical Engineering
3053 Merrill Engineering Bldg.
Salt Lake City, Utah 84112
Attn: Dr. J. Mark Baird — 1 copy

University of Wisconsin
Department of Electrical Engineering
Madison, Wisconsin, 53706
Attn: R. Vernon — 1 copy

U. S. Naval Academy
Annapolis, Maryland 21402-5021 — 1 copy

U. S. Army
Harry Diamond Labs
2800 Powder Mill Road
Adelphi, Maryland 20783-1145
Attn: Dr. Edward Brown — 1 copy
Dr. Michael Chaffey — 1 copy
Dr. Howard Brandt — 1 copy
Dr. Art Sindoris — 1 copy

U.S. Army
Armament R an D Center
Attn SMCAR-FSP-A(2)
Attn: Dr. Robert Kinasewitz — 1 copy
Stephen Saddow — 1 copy

Commander
U.S. Army VAL
Attn: SLCVA-TAC
R. Flores
White Sands Missile Range
New Mexico, 88002-5513 — 2 copies

Varian Associates
611 Hansen Way
Palo Alto, California 94303
Attn: Dr. H. Jory — 1 copy
Dr. David Stone — 1 copy
Dr. Kevin Felch — 1 copy
Dr. A. Salop — 1 copy
Dr. B. Alper — 1 copy

Varian Eimac San Carlos Division
301 Industrial Way
San Carlos, California 94070
Attn: C. Marshall Loring — 1 copy

Yale University
Applied Physics
Madison Lab
P.O. Box 2159
Yale Station
New Haven, Connecticut 06520
Attn: Dr. N. Ebrahim — 1 copy
Dr. I. Bernstein — 1 copy

Do NOT make labels for
Records------(01 cy)

Director of Research
U.S. Naval Academy
Annapolis, MD 21402

Naval Research Laboratory
Washington, DC 20375-5000
Code 2634
Timothy Calderwood